PLANT SCIENCES

A KNOTTED1-LIKE HOMEOBOX PROTEIN1–interacting transcription factor SlGATA6 maintains the auxin-response gradient to inhibit abscission

Xianfeng Liu[1,2,3], Lina Cheng[1,2,3], Yue Cai[1,2,3], Yang Liu[1,2,3], Xuemei Yan[1,2,3], Jiayun Liu[1,2,3], Ruizhen Li[1,2,3], Siqi Ge[1,2,3], Sai Wang[1,2,3], Xingan Liu[1,2,3], Sida Meng[1,2,3], Mingfang Qi[1,2,3], Cai-Zhong Jiang[4,5], Tianlai Li[1,2,3], Tao Xu[1,2,3]*

The KNOTTED1-LIKE HOMEOBOX PROTEIN1 (SlKD1) is a master abscission regulator in tomato (*Solanum lycopersicum*). Here, we identified an SlKD1-interacting transcription factor GATA transcription factor 6 (SlGATA6), which is required for maintaining the auxin-response gradient and preventing abscission. SlGATA6 up-regulates the expression of *SlLAX2* and *SlIAA3*. The AUXIN RESISTANT/LIKE AUXIN RESISTANT (AUX/LAX) proteins SlLAX2-dependent asymmetric auxin distribution causes differential accumulation of Auxin/Indole-3-Acetic Acid 3 (SlIAA3) and its homolog SlIAA32 across different abscission zone cells. It is also required for SUMOylation of AUXIN RESPONSE FACTOR 2a (SlARF2a), a key suppressor of auxin signaling and abscission initiator. Moreover, SlIAA3 and SlIAA32 depress SUMOylated SlARF2a, thus suppressing SlARF2a function. The interaction between SlKD1 and SlGATA6 suppresses SlGATA6 binding to the promoters of *SlLAX2* and *SlIAA3*, thereby disrupting the auxin-response gradient and triggering abscission. This regulatory mechanism is conserved under low light–induced abscission in diverse Solanaceae plants. Our findings reveal a critical role of SlKD1 in modulating the auxin-response gradient and abscission initiation.

INTRODUCTION

In plants, abscission usually takes place in a specific site called the abscission zone (AZ) (*1*, *2*). Auxin is an important inhibitor of abscission. Flowers and fruits are rich sources of auxin, which are transferred from these organs to other regions via AZ. This polar transport of auxin forms an auxin gradient in the AZ and thus inhibits abscission (*3*–*5*). Impairment of the continuous polar flow of auxin through the AZ abolishes the auxin-response gradient, resulting in ethylene sensitivity in the AZ cells and initiating abscission (*6*–*9*). The initiation of abscission can be triggered by developmental signals or environmental stimuli, such as darkness (*10*), low light (*11*, *12*), and drought (*13*); however, the mechanism underlying the interruption of the auxin-response gradient to initiate abscission is still obscure.

Interrupting the auxin flux by using the auxin transport inhibitor N1-naphthylphthalamic acid notably accelerates abscission (*14*). The polar auxin transporters AUXIN RESISTANT/LIKE AUXIN RESISTANT (AUX/LAX) and PIN-FORMED (PIN) are responsible for auxin influx and efflux, respectively (*15*–*17*). Down-regulating the expression of specific *AUX/LAX* or *PIN* genes causes premature abscission (*7*, *18*). The local auxin response in AZ cells is mediated by auxin signaling. The auxin-promoted degradation of Aux/IAAs (AUXIN/indole-3-acetic acids) releases the repression imposed on AUXIN-RESPONSIVE FACTOR (ARF) proteins to transcriptionally activate or repress downstream auxin-responsive genes. Different Aux/IAA-ARF modules are involved in various aspects of development (*19*–*21*). The core auxin regulatory genes involved in abscission have largely been identified. For example, in *Arabidopsis* (*Arabidopsis thaliana*), loss-of-function mutants of *ARF2* exhibit delayed abscission, suggesting that ARF2 plays a dominant role in initiating abscission (*22*, *23*). Furthermore, microarray assays in tomato indicated that *ARF* expression levels did not change during pedicel abscission induced by manual removal of flowers, suggesting that abscission is regulated in an *Aux/IAA* expression-dependent mechanism (*3*). In agreement with this idea, the expression levels of six *Aux/IAA* genes in red cestrum (*Cestrum elegans*) were negatively correlated with floret abscission (*24*). Overexpression of *axr3-1*, a gain-of-function, semidominant allele of *IAA17*, notably delayed floral organ abscission in *Arabidopsis* (*7*). Knocking down *RhIAA16* transcript levels by virus-induced gene silencing (VIGS) notably accelerated petal abscission in rose (*Rosa hybrida*), suggesting that Aux/IAAs prevent premature abscission (*25*).

In plants, C2C2-GATA-transcription factors are evolutionarily conserved transcription factors (*26*). The *GATA* genes of tomato (*Solanum lycopersicum*), *Arabidopsis*, and rice (*Oryza sativa*) can be divided into four subfamilies (I to IV) (*26*, *27*). Members from subfamily I have been reported to participate in auxin signaling. For instance, *Arabidopsis* GATA2 restricts cell division involved in auxin-mediated root elongation, and the overexpression of its encoding gene decreased β-glucuronidase (GUS) activity derived from a *DR5:GUS* transgene in roots by down-regulating the expression of *PIN1* and a suite of auxin-response genes (*28*). Posttranscriptional regulation also modulates GATA function. For example, darkness induces the proteasomal degradation of *Arabidopsis* GATA2 in a CONSTITUTIVE PHOTOMORPHOGENIC 1 E3 ubiquitin ligase–dependent manner to prevent photomorphogenesis (*29*). In tomato, the basic leucine zipper transcription factor LONG HYPOCOTYL 5 interacts with SlGATA17 and suppresses *SlGATA17* expression to regulate seed germination during stress (*30*). However, whether

[1]College of Horticulture, Shenyang Agricultural University, Shenyang, Liaoning 110866, China. [2]Key Laboratory of Protected Horticulture of Ministry of Education, Shenyang, Liaoning, China. [3]Modern Protected Horticulture Engineering and Technology Center, Shenyang Agricultural University, Shenyang 110866, China. [4]Crops Pathology and Genetic Research Unit, United States Department of Agriculture Agricultural Research Service, Davis, CA 95616, USA. [5]Department of Plant Sciences, University of California at Davis, Davis, CA 95616, USA.
*Corresponding author. Email: syauxutao@syau.edu.cn

GATAs contribute to auxin signaling in the context of plant abscission and their underlying regulatory mechanisms are still unknown.

KNOX proteins comprise a small family of homeobox proteins with three–amino acid loop extensions and can be divided into three subclasses: I, II, and M (*31*). In tomato, three *KNOX* genes, *TOMATO KNOTTED3* (*TKN3*), *TNK4*, and *KNOTTED1-LIKE HOMEOBOX PROTEIN1* (*KD1*), are strongly expressed in the AZ of pedicels connecting the fruits and the plant (*32*). In our previous study, we reported that several transcription factors, WUSCHEL (WUS), KD1, and FRUTFULL 2 (FUL2), participate in low light– and auxin depletion–induced abscission (*12*). Genetic evidence indicated that SlWUS acted upstream of SlKD1 to regulate these two types of abscissions. Several studies have demonstrated that SlKD1 modulates the auxin concentration and response gradient in the AZ and plays a critical role in initiating abscission (*12*, *32*, *33*). However, the class M KNOX protein SlKD1 lacks a clear DNA-binding homeodomain, suggesting that SlKD1-mediated abscission might depend on other proteins that bind to DNA.

Here, we identified SlGATA6 as interacting with SlKD1; this interaction suppresses the binding of SlGATA6 to the *SlLAX2* and *SlIAA3* promoters and inhibits their transcription. We provide evidence that the auxin gradient, established by SlLAX2, stabilizes the noncanonical AUX/IAA protein SlIAA32, which interacts and inhibits SlARF2a, a major player in abolishing the auxin-response gradient across the AZ, thus accelerating abscission, together with SlIAA3. Together, our results describe a molecular mechanism whereby auxin depletion– and low light–induced *SlKD1* expression breaks the auxin-response gradient and initiates abscission.

RESULTS

SlKD1 directly interacts with SlGATA6

We previously showed that SlKD1 influences the auxin-response gradient and auxin concentration to enhance abscission inside the AZ (*12*, *32*). However, because SlKD1 lacks a DNA-binding homeodomain, SlKD1-mediated abscission is likely to require other proteins that bind to DNA. To identify the possible regulatory proteins interacting with SlKD1, we performed a yeast two-hybrid (Y2H) screen using a cDNA library prepared from total RNA extracted from tomato flower AZs at different times following flower removal (0, 2, 4, 8, 12, and 16 hours). Among 17 independent candidate interactors, we noticed a GATA transcription factor, SlGATA6 (Fig. 1A and data S1). Phylogenetic analysis suggested that SlGATA6 belongs to subfamily I and is most closely related to *Arabidopsis* GATA6 (fig. S1A). A subcellular localization assay indicated that a SlGATA6–green fluorescent protein (GFP) fusion accumulates in the nucleus (fig. S1B). To determine which regions of SlKD1 and SlGATA6 interact in yeast, we divided SlKD1 into two fragments and SlGATA6 into three based on their conserved functional domains (Fig. 1B). We observed an interaction between the C terminus of SlKD1 containing the KNOX2 domain and the C-terminal ZnF domain of SlGATA6 (Fig. 1C). We validated this interaction in vitro by performing a pull-down assay with recombinant full-length SlKD1-His and SlGATA6 fused to glutathione *S*-transferase (SlGATA6-GST), as well as with truncated $SlKD1_C$-His and $SlGATA6_C$-GST (Fig. 1, D and E). To validate their interaction in vivo, we performed coimmunoprecipitation (co-IP) assays by coexpressing *SlKD1-Flag* (encoding SlKD1 with a Flag tag) and *SlGATA6-GFP* in *Nicotiana benthamiana* leaves, which revealed that SlGATA6 associates with SlKD1 in plant cells (Fig. 1F). A bimolecular fluorescence complementation (BiFC) assay indicated that the SlKD1-SlGATA6 interaction occurs in the nucleus. Deleting the C-terminal region of SlKD1 ($SlKD1_{\Delta C}$) or the C terminus of SlGATA6 ($SlGATA6_{\Delta C}$), which were both critical for their interaction in yeast, abolished the SlKD1-SlGATA6 interaction in plant cells (Fig. 1G). These results indicate that SlGATA6 directly interacts with SlKD1.

SlGATA6 plays a negative role in flower pedicel abscission

A reverse-transcription quantitative PCR (RT-qPCR) assay indicated that *SlGATA6* is abundantly expressed in the AZ of flower pedicels at time 0 hours before flower removal (fig. S1C); we obtained independent support of this claim by RNA in situ hybridization using a specific antisense probe for *SlGATA6* transcripts (Fig. 1H). *SlGATA6* expression decreased quickly before remaining at a low level following flower removal, which induces pedicel abscission caused by auxin depletion (fig. S1D). To understand the function of SlGATA6 in abscission, we generated *SlGATA6* loss-of-function mutants using CRISPR-Cas9 gene editing and *SlGATA6* overexpression (*SlGATA6*-OE) lines (fig. S1, E to G). We observed accelerated abscission of the pedicel in three independent *Slgata6* mutant lines and delayed abscission in *SlGATA6*-OE lines compared to wild-type (WT) plants after flower removal (Fig. 1I). These results confirm that SlGATA6 inhibits flower pedicel abscission.

RNA-seq analysis shows that SlGATA6 regulates auxin-related pathways

To investigate the mechanisms underlying the accelerated abscission in the *Slgata6* mutants, we explored differential gene expression in the AZ at 4 hours after flower removal between WT and *Slgata6* plants by transcriptome deep sequencing [RNA sequencing (RNA-seq)]. We identified 1316 significantly differentially expressed genes [DEGs; absolute $|\log_2$ fold-change$| \geq 1$, false discovery rate (FDR) <0.01] in *Slgata6* plants compared to WT plants, of which 429 were up-regulated genes and 887 were down-regulated genes (fig. S2A and data S2). A Kyoto Encyclopedia of Genes and Genomes (KEGG) pathway enrichment analysis to classify the top 10 significant pathways enriched in DEGs determined that the "plant hormone signal transduction pathway" is the most enriched (Fig. 2A). A closer look at the enriched DEGs in the plant hormone signal transduction pathway revealed that these genes are responsible for auxin homeostasis and signaling (26 out of 33, data S3). The down-regulated genes encode 13 AUX/IAA proteins, one ARF-type transcription factor, three SMALL AUXIN-UPREGULATED RNAs (SAURs), one auxin transporter (LAX2), and five GRETCHEN HAGEN3s (GH3s); genes encoding a SAUR and two GH3s were up-regulated (Fig. 2B). To validate the data from the RNA-seq analysis, we measured the relative transcript levels of six auxin-related genes using RT-qPCR (fig. S2B). The changes in gene expression seen using RNA-seq and RT-qPCR were consistent for all six genes, confirming the validity of the RNA-seq data.

SlGATA6 regulates auxin-related genes by binding to their promoters

To define the specific target genes directly regulated by SlGATA6, we used DNA affinity purification sequencing (DAP-seq), which is an in vitro DNA-binding assay used to globally capture the DNA-binding sites of a given transcription factor in the genomic context (*34*). We obtained 34,707 highly reliable SlGATA6-binding peaks, of which

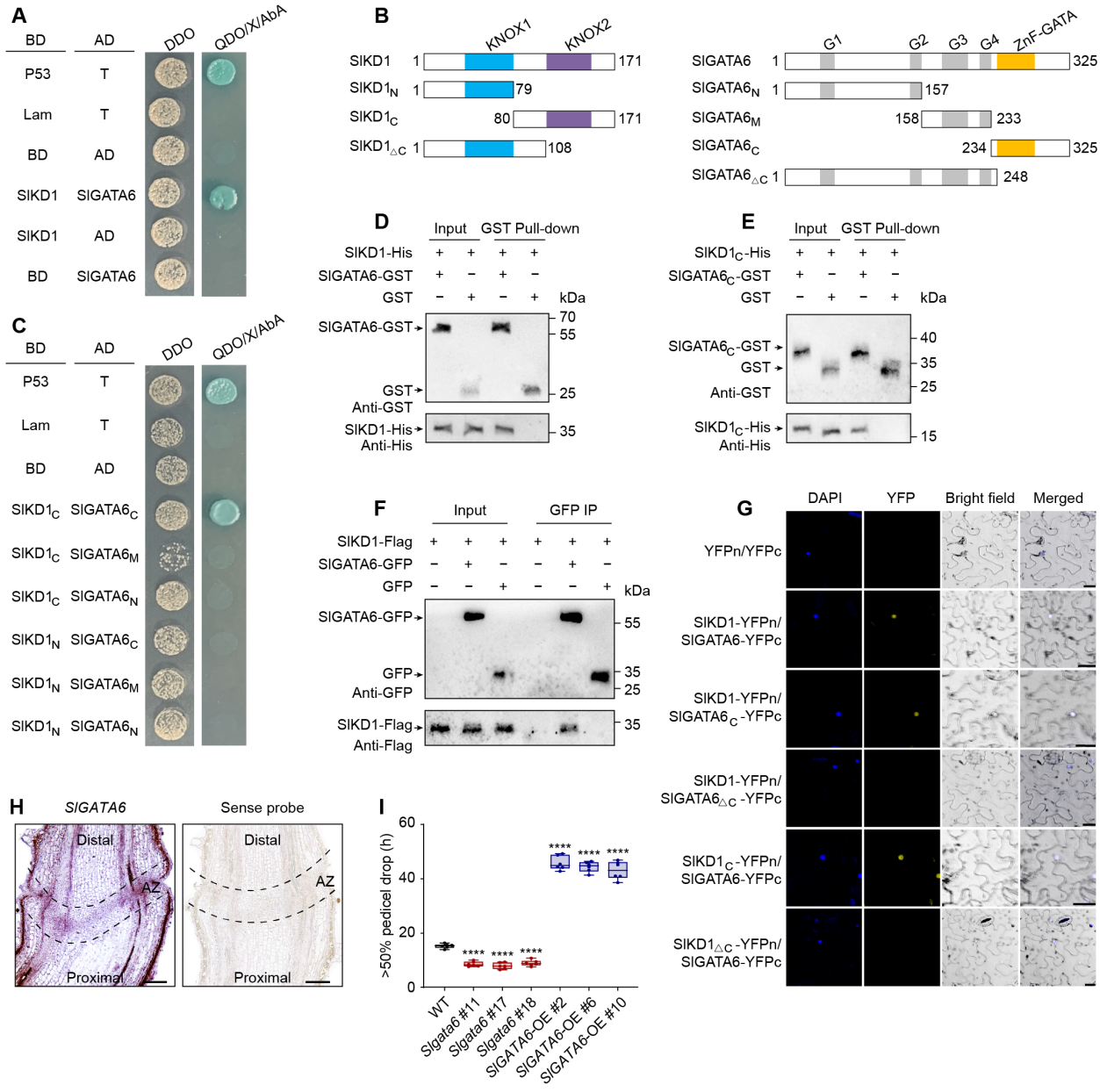

Fig. 1. SlGATA6 interacts with SlKD1 and inhibits abscission. (**A**) Y2H assay showing that SlKD1 interacts with SlGATA6. *SlKD1* was cloned into the pGBKT7 vector [with GAL4 DNA-binding domain (BD)]; *SlGATA6* was ligated into the pGADT7 vector [with GAL4 activation domain (AD)]. DDO, double dropout medium (synthetic defined medium lacking Trp and Leu). QDO, quadruple dropout medium (synthetic defined medium lacking Trp, Leu, His, and Ade). X, X-a-gal. AbA, Aureobasidin A. (**B**) Diagrams of full-length and various truncated forms of SlKD1 and SlGATA6 used in (C), (E), and (G). KNOX, KNOTTED1-like homeobox domain. G1 to G4, GATA low complexity domains. ZnF-GATA, zinc-finger DNA-binding domain. Numbers denote amino acids. (**C**) Y2H assay showing that $SlKD1_C$ directly interact with $SlGATA6_C$. (**D**) Pull-down assays of the interaction between full-length SlKD1 and SlGATA6. (**E**) Pull-down assays for SlKD1 and SlGATA6 fragments interaction. (**F**) Immunoprecipitation assay showing the interaction of SlKD1 with SlGATA6 in vivo. *SlKD1*-Flag was coexpressed with *SlGATA6*-GFP or GFP in *N. benthamiana* leaves. Protein complexes were immunoprecipitated using GFP beads and analyzed by immunoblot. (**G**) BiFC assays showing the interaction between SlKD1 and SlGATA6 *in planta*. DAPI, 4′,6-diamidino-2-phenylindole; YFP, yellow fluorescent protein. Scale bars, 25 μm. (**H**) RNA in situ hybridization for *SlGATA6* transcripts in flower pedicels. The sense probe was used as a negative control. AZ, abscission zone. Scale bars, 200 μm. (**I**) Number of hours required to achieve 50% pedicel abscission in the WT, *Slgata6*, and *SlGATA6*-OE plants. Boxplots present data of six independent tests with at least 15 pedicels in each. Significant differences were determined by one-way analysis of variance (ANOVA) with Dunnett's test compared to the WT; ****$P < 0.0001$. Box plot shows maxima, first quartile, median, third quartile, and minima. h, hours.

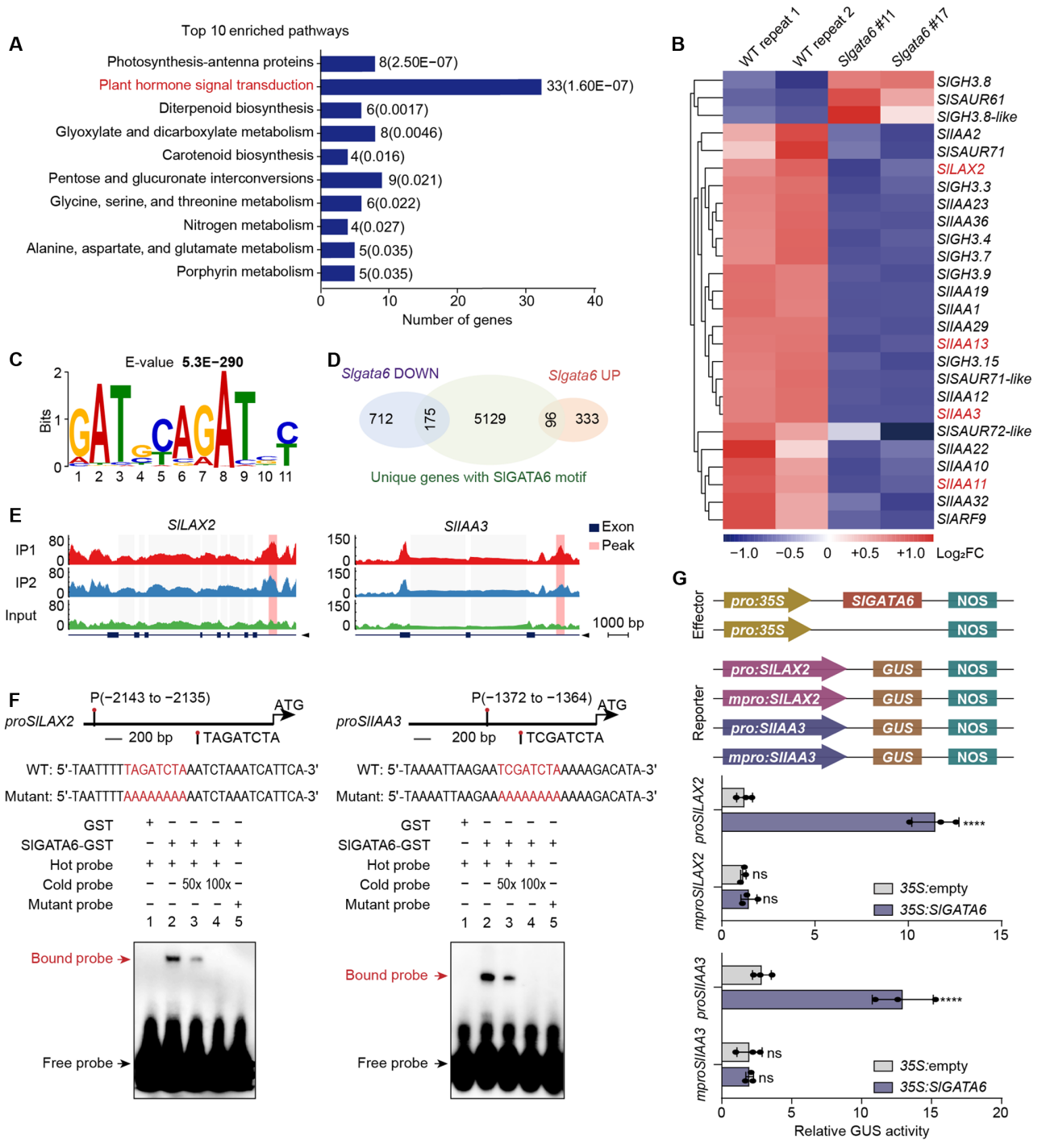

Fig. 2. SlGATA6 positively and directly regulates the expression of auxin-related genes. (**A**) KEGG pathway enrichment analysis of DEGs as determined by RNA-seq analysis of AC and *Slgata6* AZs. The numbers in parentheses mean *P* values. (**B**) Heatmap representation of auxin-related DEGs in WT and *Slgata6*. Relative mRNA expression levels (reads per kilobase per million reads) in RNA-seq data from two biological replicates were used for the analysis using TBtools (*62*). (**C**) Sequence logo showing the SlGATA6 DNA-binding motif. (**D**) Venn diagram showing the extent of overlap between SlGATA6-bound genes and up-regulated and down-regulated genes in *Slgata6* AZs. (**E**) Genome browser windows of SlGATA6-bound loci *SlLAX2* and *SlIAA3*, showing the distribution of reads obtained by DAP-seq. The DAP-seq reads are color coded: green denotes the input reads; red and blue, the two replicates for SlGATA6-bound reads; the peak position is indicated by the red shaded area. (**F**) EMSAs using probes from the *SlLAX2* and *SlIAA3* promoters demonstrating that recombinant SlGATA6-GST binds to the *SlIAA3* and *SlLAX2* promoters. Red letters indicate the SlGATA6 binding motif identified by DAP-seq or its mutated variant used in the mutant probes. (**G**) Promoter assays showing that SlGATA6 activates the transcription of *SlIAA3* and *SlLAX2*. *SlIAA3* and *SlLAX2* promoters were cloned upstream of the *GUS* reporter gene. *N. benthamiana* leaves were coinfiltrated with the *GUS* reporter constructs containing either the intact *SlLAX2* or *SlIAA3* promoters (*pro*) or mutant variants (*mpro*) harboring mutations in the SlGATA6-binding site and the *35S:SlGATA6* effector construct or empty vector (control). The values are means ± SD from three biological replicates. One-way ANOVA with Tukey's test was used to assess statistical significance relative to *35S*:empty; ****$P < 0.0001$; ns, no significant difference.

~33.2% were located upstream from transcription start sites (≤2.5 kb upstream of the start codon, fig. S2C). KEGG enrichment analysis established that these putative SlGATA6 target genes are mainly enriched in pathways related to "biosynthesis of secondary metabolites" and "plant hormone signal transduction" (fig. S2D). We identified a total of 19,096 highly reliable SlGATA6-binding sites located within the regulatory regions of 5400 genes (data S4). The consensus sequence for the SlGATA6 binding motif was GAT(G/C)CAGAT(C/G)(C/T) (Fig. 2C). Notably, this motif includes the core sequence GATC, a previously identified GATA6 recognition motif in *Arabidopsis* (*35*).

We compared the 1316 DEGs derived from the RNA-seq analysis to the above 5400 SlGATA6-bound genes from our DAP-seq data to identify those direct SlGATA6-regulated target genes. In total, 271 genes (175 down-regulated and 96 up-regulated) were shared by the DAP-seq and RNA-seq datasets, suggesting that they are direct targets of SlGATA6 (Fig. 2D and data S5); about 20.6% of the DEGs (271 of 1316) contained the SlGATA6-binding site in their regulatory regions. Among the 271 overlapping genes, we focused on 4 genes involved in the auxin pathway: 3 *AUX/IAA* genes (*SlIAA3*, *SlIAA11*, and *SlIAA13*) and 1 auxin transporter gene (*SlLAX2*) (Fig. 2E and fig. S3, A and B), down-regulated in *Slgata6* plants and whose promoters were bound by SlGATA6 (Fig. 2B).

To validate the binding of SlGATA6 to the promoters of these four auxin-related genes, we turned to electrophoretic mobility shift assays (EMSAs). Recombinant SlGATA6-GST showed direct binding to probes derived from all four auxin-related genes and containing the predicted SlGATA6-binding site (Fig. 2F and fig. S3, C and D). To determine how SlGATA6 regulates these four genes, we used a β-GLUCURONIDASE (GUS) transactivation assay in *N. benthamiana* leaves. When the *35S:SlGATA6* effector construct was coinfiltrated with the intact promoter reporter constructs for *SlLAX2*, *SlIAA3*, *SlIAA11*, or *SlIAA13*, we observed an increase in relative GUS activity, but not with mutated versions (all bases mutate into A) of these promoters with a mutation in the predicted SlGATA6-binding site (Fig. 2G and fig. S3E). These findings demonstrate that SlGATA6 activates the transcription from the *SlLAX2*, *SlIAA3*, *SlIAA11*, and *SlIAA13* promoters.

SlLAX2 delays abscission by affecting auxin concentration across AZ

To explore their effects on abscission, we used VIGS to produce individual tomato plants knocked down for *SlLAX2*, *SlIAA3*, *SlIAA11*, or *SlIAA13*. Silencing *SlLAX2* or *SlIAA3* resulted in accelerated abscission, while silencing *SlIAA11* or *SlIAA13* had no significant effect on abscission (fig. S4). To eliminate the redundant functions of *SlIAAs*, we conducted concurrent silencing of *SlIAA3* and *SlIAA11*, *SlIAA3* and *SlIAA13*, *SlIAA11* and *SlIAA13*, and also silenced all three *SlIAAs* simultaneously to investigate their functional roles. Only SlIAA3 was involved in abscission (fig. S5). We further detected the expression levels of *SlLAX2* and *SlIAA3* in WT and *SlGATA6* mutants by RT-qPCR and found that the expression levels of *SlLAX2* and *SlIAA3* were significantly down-regulated in mutants compared with WT (fig. S6). Therefore, we chose *SlLAX2* and *SlIAA3* for further characterization.

We first explored the roles of SlLAX2 in establishing the auxin concentration in the AZ, as LAXs are involved in local auxin accumulation (*15*). RT-qPCR analysis and RNA in situ hybridization assays indicated that *SlLAX2* transcripts are abundant in the AZ at time 0 hours before flower removal (fig. S7, A to C). Moreover, *SlLAX2* expression sharply decreased following flower removal (fig. S7D), similar to *SlGATA6* expression (fig. S1D). When we generated knockout mutant lines for *SlLAX2* using CRISPR-Cas9 and *SlLAX2* overexpression lines (fig. S7, E to G), we determined that *Sllax2* plants exhibit significantly accelerated abscission, while *SlLAX2*-OE lines had significantly delayed abscission compared to the WT (Fig. 3A). Knockout of *SlLAX2* significantly decreased the auxin concentration in the AZ compared to that in the WT; by contrast, the auxin concentration was significantly higher in *SlLAX2*-OE lines than in the WT (Fig. 3B). To examine auxin signaling output in the pedicel, we used *DR5:GUS* lines in which *GUS* is driven by the auxin-responsive synthetic promoter element DR5 (*12*, *32*, *36*). We introduced the *DR5:GUS* transgene into the *Sllax2* lines by crossing and stained the pedicels of *Sllax2 DR5:GUS* plants to reveal GUS activity. We detected little GUS staining in the region proximal to the AZ or within the AZ itself, in contrast to *DR5:GUS* plants in the AC background, indicating that loss of SlLAX2 function results in a lower auxin signaling output across the pedicel (Fig. 3C). These results indicate that SlLAX2-dependent auxin influx is important for auxin accumulation in the AZ, which inhibits abscission.

SlLAX2-dependent auxin concentration stabilizes SlIAA32 to maintain auxin-response gradient

Aux/IAA proteins commonly harbor four conserved amino acid sequence patterns, referred to as domains I, II, III, and IV. The F-box protein TRANSPORT INHIBITOR RESPONSE 1 (TIR1) interacts with domain II of Aux/IAAs in an auxin-dependent manner and leads to the destabilization of Aux/IAA proteins (*37*, *38*). Noncanonical AUX/IAAs lack the canonical domain II and cannot be degraded by the TIR1 complex. However, high concentrations of auxin can stabilize noncanonical AUX/IAAs to mediate a local auxin response (*20*, *38*). High concentrations of auxin activate TRANSMEMBRANE KINASE 1 (TMK1) at the cell surface and lead to the cleavage of the TMK1 C terminus in *Arabidopsis* (*20*). Phosphorylation of the noncanonical Aux/IAAs IAA32 and IAA34 by the TMK1 C-terminal domain enhances IAA32 and IAA34 protein stability and plays an important role in apical hook formation (*20*). SlIAA32 and SlIAA33 are noncanonical AUX/IAAs in tomato (*39*), but only *SlIAA32* was highly expressed in the AZ (fig. S8A). RNA in situ hybridization indicated that *SlIAA32* transcripts are abundant in the AZ (fig. S8, B and C). Furthermore, cell-free degradation assays indicated that auxin treatment enhances the stability of SlIAA32, while application of the auxin biosynthesis inhibitor L-kynurenine (L-Kyn) decreased its stability (Fig. 3D). Relative *SlIAA32* transcript levels were similar in WT, *SlLAX2*-OE, and *Sllax2* plants (fig. S8D); however, SlIAA32 accumulated to higher levels in *SlLAX2*-OE lines and to lower levels in *Sllax2* lines compared to the WT, indicating that SlIAA32 may be more stable in *SlLAX2*-OE lines and less stable in *Sllax2* lines (Fig. 3E).

Knockout of *SlIAA32* significantly accelerated abscission compared to that in the WT (fig. S8E and Fig. 3F). The auxin-response gradient was much weaker in *Sliaa32* mutant lines than in the WT, as indicated by the *DR5:GUS* reporter (Fig. 3C). In addition, while exogenous application of the synthetic auxin naphthaleneacetic acid (NAA) to treat the flower pedicel of WT and *Sliaa32* mutant lines, we found that *Sliaa32* mutants were less sensitive to auxin treatment, reaching a higher abscission rate than WT at the same period (fig. S8F). We crossed *SlLAX2*-OE to *Sliaa32* and established that *Sliaa32 SlLAX2*-OE plants display increased abscission compared to *SlLAX2*-OE (Fig. 3G). These results demonstrate that SlLAX2-dependent auxin

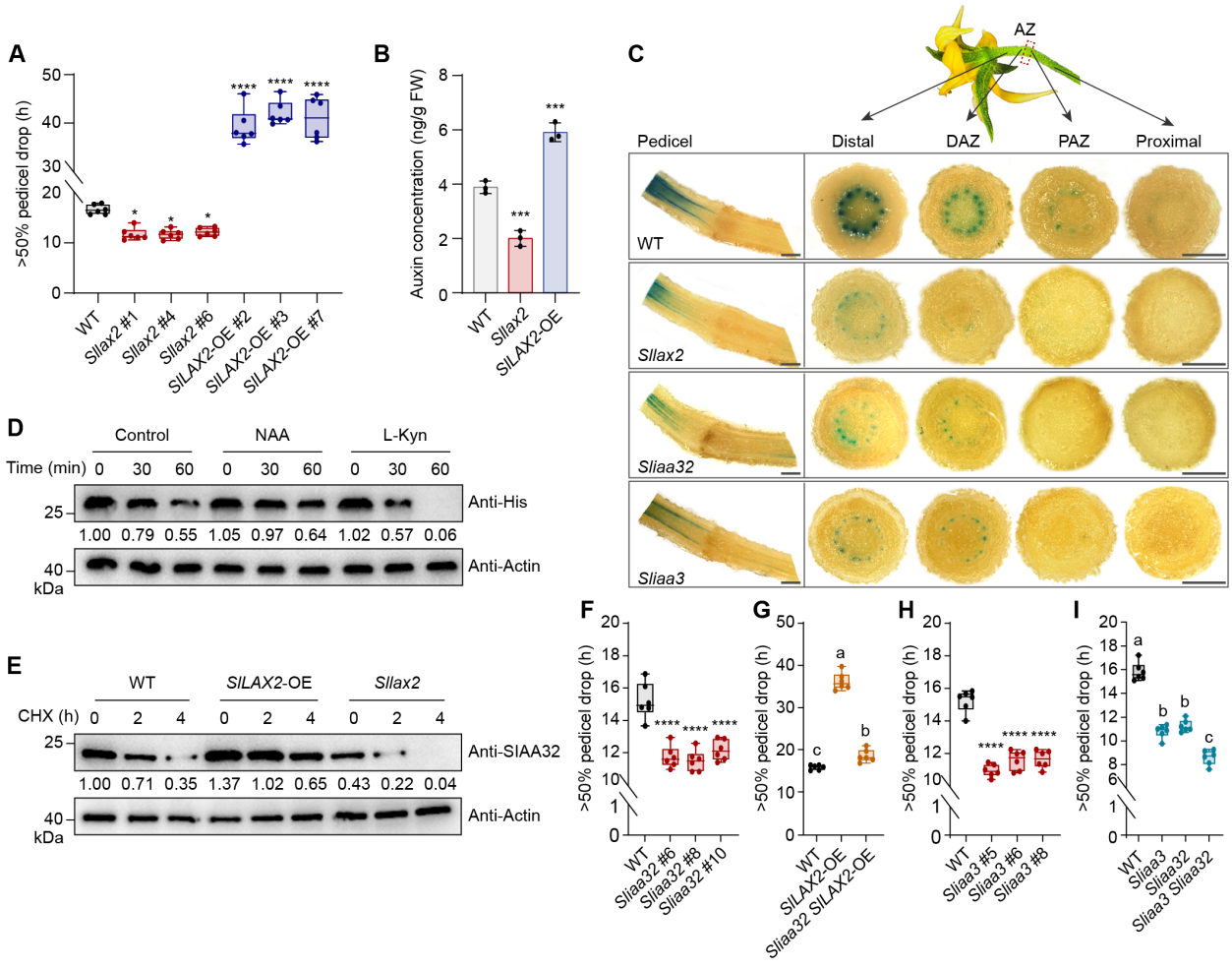

Fig. 3. SlLAX2, SlIAA3, and SlIAA32 suppress tomato pedicel abscission. (**A**) Number of hours required for WT, *Sllax2*, and *SlLAX2*-OE plants to achieve 50% pedicel abscission. (**B**) Auxin contents in the AZ of WT, *Sllax2*, and *SlLAX2*-OE plants. The values are means ± SD from three biological replicates. (**C**) GUS staining pattern derived from *DR5:GUS* reporter in the AZ of WT, *Sllax2*, *Sliaa32*, and *Sliaa3* plants. Transverse sections were made from distal region, distal side of the AZ (DAZ), proximal side of the AZ (PAZ), and proximal region, as indicated. Images were digitally extracted for comparison. Three independent plant specimens were used, each with at least 10 pedicels. Scale bars, 1 mm. (**D**) Cell-free degradation test to examine the influence of naphthaleneacetic acid (NAA) or L-kynurenine (L-Kyn) treatment on SlIAA32 degradation. Equal amounts of recombinant SlIAA32-His were incubated with total protein extracts from WT AZs treated with water (control), NAA, or L-Kyn for 30 or 60 min. The presence of SlIAA32 was determined using an anti-His antibody. Actin as a loading control. (**E**) In vivo degradation assay of SlIAA32 in WT, *SlLAX2*-OE, and *Sllax2* plants. The pedicel AZs were treated with 100 μM cycloheximide (CHX) for different times. (**F** to **I**) Number of hours required for the WT and *Sliaa32* lines (F), *SlLAX2*-OE and *Sliaa32 SlLAX2*-OE (G), WT and *Sliaa3* lines (H), and *Sliaa3*, *Sliaa32*, and *Sliaa3 Sliaa32* (I) plants to achieve 50% pedicel abscission. Significant differences were determined by one-way ANOVA with Tukey's test [(A), (G), (H), and (I)] or Dunnett's test [(B) and (F)]; $*P < 0.05$, $***P < 0.001$, $****P < 0.0001$; different lowercase letters indicate significant differences ($P < 0.05$). Boxplots show data from six independent replicates, each consisting of at least 15 pedicels, with maxima, first quartile, median, third quartile, and minima. h, hours.

concentration functions upstream of SlIAA32 to maintain the auxin-response gradient across the AZ and inhibit abscission.

SlIAA3 delays abscission and functions independently of SlIAA32

We explored the roles of SlIAA3 in the AZ, as AUX/IAAs are involved in auxin signaling. RT-qPCR analysis and RNA in situ hybridization assays indicated that *SlIAA3* is abundantly expressed in the AZ at time 0 hours before flower removal (fig. S9, A to C), with *SlIAA3* expression sharply decreasing following flower removal (fig. S9D). We knocked out *SlIAA3* by CRISPR-Cas9 and found that, compared to the WT, knockout of *SlIAA3* significantly accelerates abscission (Fig. 3H and fig. S9E). *Sliaa3 DR5:GUS* plants also showed a severely impaired auxin-response gradient with almost no GUS staining detected in the AZ or proximal regions (Fig. 3C). These results indicate that SlIAA3-dependent auxin signaling is important for forming the auxin-response gradient to prevent abscission.

To further explore the relationship between SlIAA32 and SlIAA3 in mediating abscission, we generated the *Sliaa3 Sliaa32* double mutant by genetic crossing of two single mutants. *Sliaa3 Sliaa32* plants had higher abscission levels than the respective *Sliaa3* and *Sliaa32* single mutants, indicating that SlIAA32 and SlIAA3 nonredundantly prevent abscission (Fig. 3I).

SlIAA3/SlIAA32 delay abscission by directly interacting with SUMOylated SlARF2a

Aux/IAAs primarily block the function of ARFs in the auxin signaling cascade (*37*, *40*, *41*). To determine which ARFs are repressed by

SlIAA3 and SlIAA32 during tomato flower pedicel abscission, we assessed SlARF protein abundance in the AZ using liquid chromatography–tandem mass spectrometry (LC-MS/MS). We detected four SlARFs (SlARF2a, SlARF4, SlARF6, and SlARF14) in the AZ (data S8). To determine their potential effect on abscission, we used VIGS to knock down the transcript levels of each *SlARF* gene individually and monitored the abscission rate in the resulting knockdown plants. Only the *SlARF2a*-VIGS plants showed delayed abscission relative to the WT, whereas the other VIGS plants had no effect (fig. S10). RT-qPCR analysis and RNA in situ hybridization assays indicated that *SlARF2a* is abundantly expressed in the AZ at time 0 hours before flower removal (fig. S11, A to C). Furthermore, knockout of *SlARF2a* by CRISPR-Cas9 significantly delayed abscission, while *SlARF2a* overexpression lines showed accelerated abscission (Fig. 4A and fig. S11, D to F), demonstrating that SlARF2a promotes abscission. SlARF2a is a core positive regulator of ethylene signaling during tomato fruit ripening (*42*). We found that after ethylene treatment, compared with WT plants, the tomato pedicel explants of *Slarf2a* plants exhibited a significant delay in abscission (fig. S11G), indicating that SlARF2a is the key factor for the AZ to respond to ethylene and promote abscission. We also introduced the *DR5:GUS* reporter into *SlARF2a*-OE lines by crossing and found that *SlARF2a* overexpression strongly impairs the auxin-response gradient (fig. S11H), similar to the *Sliaa3* and *Sliaa32* lines (Fig. 3C), indicating that *SlARF2a* is a powerful auxin-response depressor. On the basis of these results, we speculate that SlIAA3 and SlIAA32 inhibit abscission by repressing SlARF2a function; however, SlIAA3 and SlIAA32 failed to interact with SlARF2a in a Y2H assay (fig. S11I).

In *Arabidopsis*, the interaction between ARF7 and IAA3 is dependent on the small ubiquitin-like modifier molecule SUMO for the regulation of root branching toward water (*43*). Bioinformatics analysis revealed that SlARF2a contains three putative SUMOylation sites, namely, at lysine residues K104, K686, and K632 (Fig. 4B); in addition, SlIAA3 and SlIAA32 contain a SUMO-interaction motif (SIM) (Fig. 4C). We therefore tested whether SlIAA3 and SlIAA32 interact with SlARF2a in a SUMO-dependent manner.

We confirmed that SlARF2a is a target for SUMOylation by coexpressing *SlARF2a-Flag* and *SUMO-HA* (encoding SUMO with a HA tag) in *N. benthamiana* leaves; mutating the three potential SlARF2a SUMOylatable motifs from lysine to arginine (non-SUMOylatable SlARF2a$^{3K/R}$) prevented the addition of SUMO onto SlARF2a (Fig. 4D). To test the effect of SlARF2a SUMOylation on the auxin-response gradient and abscission, we expressed SUMOylatable *SlARF2a* and non-SUMOylatable *SlARF2a*$^{3K/R}$ in the *Slarf2a* background under the control of the *SlARF2a* promoter. SlARF2a$^{3K/R}$ had a greater ability to impair the auxin-response gradient and induce abscission than intact SUMOylatable SlARF2a (Fig. 4E). Using *SlARF2a*-Flag plants, we determined that flower removal represses SlARF2a SUMOylation, while exogenous application of NAA promoted SlARF2a SUMOylation (Fig. 4F). In agreement with this result, we detected much less SUMOylated SlARF2a in *Sllax2* than in the WT (Fig. 4G). These results indicate that SlLAX2-dependent auxin concentration is important for SlARF2a SUMOylation, which is required for maintaining the auxin-response gradient and preventing abscission.

Co-IP assays in *N. benthamiana* leaves indicated that SUMOylated SlARF2a interacts with SlIAA3 and SlIAA32, while non-SUMOylatable SlARF2a$^{3K/R}$ failed to do so (Fig. 4, H and I). Coexpressing SlIAA3 or SlIAA32 in combination with SlARF2a-Flag and SUMO-HA in *N. benthamiana* does not affect the SUMOylation of SlARF2a (fig. S11J). Furthermore, mutant variants of SlIAA3 and SlIAA32 with mutations in the SIM domain no longer interacted with SlARF2a (Fig. 4, H and I), underscoring the importance of SlARF2a SUMOylation in the SlARF2a-SlIAA3/SlIAA32 interaction.

As domain II is responsible for Aux/IAA stability, and an amino acid substitution in domain II can stabilize the protein (*20*, *38*), we generated a dexamethasone-inducible transgenic line for inducible expression of *SlIAA3*$_{dIIm}$ (with the domain II of SlIAA3 mutated) (*44*), *SlIAA3*$_{dIImSIMm}$ (with the domain II and SIM domains of SlIAA3 mutated), *SlIAA32*, and *SlIAA32*$_{SIMm}$ (with the SIM domain of SlIAA32 mutated) (*43*) (fig. S11, K to N). While mutating the SIM domain of SlIAA3 and SlIAA32 had little effect on abscission, the dexamethasone-induced expression of *SlIAA3*$_{dIIm}$ or *SlIAA32* delayed abscission (Fig. 4, J and K). Moreover, overexpression of *SlIAA3*$_{dIImSIMm}$/*SlIAA32*$_{SIMm}$ failed to restore the mutant phenotype in the backgrounds of *Sliaa3* and *Sliaa32* mutants (Fig. 4, L and M). All these results demonstrate the importance of the SIM domain in inhibiting abscission.

We then crossed *Slarf2a* to *Sliaa3 DR5:GUS* and *Sliaa32 DR5:GUS* plants and stained for GUS activity in pedicels. Knockout of *SlARF2a* in the *Sliaa3* and *Sliaa32* single mutant backgrounds strongly enhanced the auxin response across the AZ (fig. S11H) and resulted in a delayed abscission phenotype (Fig. 4, N and O). These results indicate that SlIAA3 and SlIAA32 negatively regulate SlARF2a function by interacting with SUMOylated SlARF2a to maintain the auxin-response gradient and prevent abscission.

SlGATA6 establishes auxin-response gradient across AZ

To explore the role of SlGATA6 in auxin homeostasis and signaling during abscission, we measured the auxin content in the AZ of WT, *Slgata6*, and *SlGATA6*-OE lines. Compared to the WT, knockout and overexpression of *SlGATA6* decreased and increased auxin levels in the AZ, respectively (fig. S12A). Moreover, following treatment with NAA (50 ng·g^{-1}), which erased the difference in the auxin concentration among the different lines, the abscission rate of *Slgata6* plants remained higher than that of the WT, but *SlGATA6*-OE plants showed a much delayed abscission rate (fig. S12B). In addition, *Slgata6 DR5:GUS* plants displayed a severely compromised auxin-response gradient, with almost undetectable GUS staining in the proximal region of the AZ and the AZ (fig. S12C). These results indicate that both the auxin concentration and response are regulated by SlGATA6.

Auxin, SlIAA3, and SlIAA32 distribution is tightly regulated by SlGATA6

To gain insight into the role of SlGATA6 in establishing the distribution of auxin, SlIAA3, and SlIAA32 in the AZ, we investigated where auxin accumulated in the pedicel AZ by immunolocalization on longitudinal pedicel sections with a monoclonal anti-IAA antibody (*45*). The cellular auxin concentration was high in distal regions and the AZ proper, while weaker in proximal AZ regions (Fig. 5, A and C). We used Calcofluor white (CFW, cell wall dye) to distinguish individual cells and made transverse sections to further study the distribution of auxin (Fig. 5, B, D, and E). Compared with the proximal side of AZ cells, there are more cells containing high auxin signal in the distal region, but not higher signal in the cell of distal region; thus, an auxin gradient with a higher concentration at the distal end and a lower concentration at the proximal end is formed in the AZ. Knockout of *SlGATA6* largely abolished the auxin gradient from the distal to proximal AZ regions,

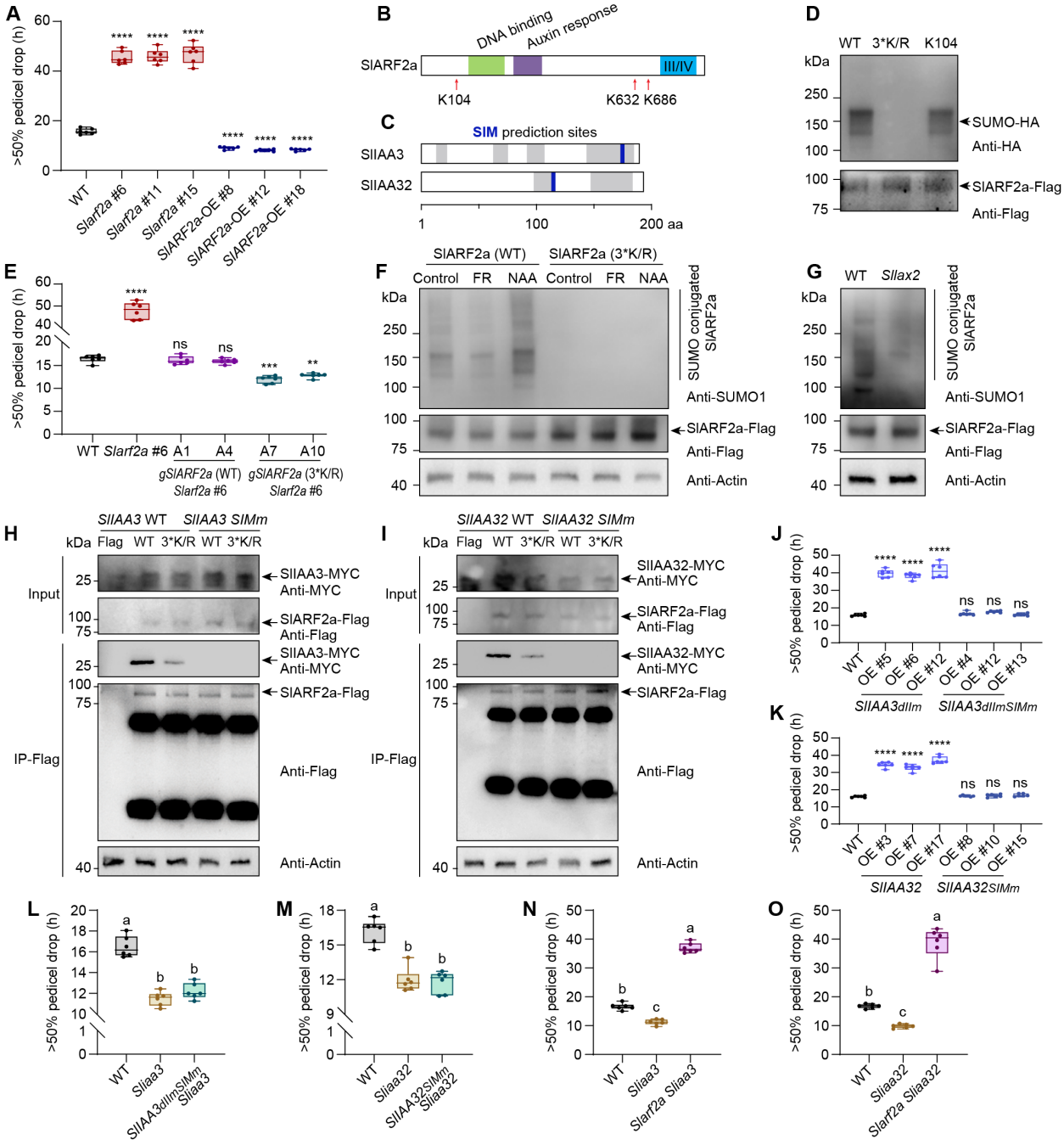

Fig. 4. SlIAA3 and SlIAA32 interact with SlARF2a in a SUMO-dependent manner to delay abscission. (**A**) Number of hours required for WT, *Slarf2a*, and *SlARF2a*-OE plants to achieve 50% abscission. (**B**) Diagram of SlARF2a domains and three predicted SUMOylated sites. (**C**) Diagrams of SlIAA3 and SlIAA32 showing putative SIMs. (**D**) Transient expression showing that mutating all SlARF2a SUMOylatable lysine sites to arginine residues in SlARF2a-Flag (3*K/R) inhibits SUMOylation with SUMO1-HA but not for WT SlARF2a or single K104R mutant. (**E**) Number of hours required for WT, *Slarf2a* #6, *Slarf2a* #6 *gSlARF2a* (WT), and *Slarf2a* #6 *gSlARF2a* (3*R/K) plants to achieve 50% abscission. (**F**) Immunoprecipitation (Anti-Flag) reveals that auxin treatment induces SUMOylation of SlARF2a-Flag but not SlARF2a-Flag (3*K/R), while auxin depletion decreases SUMOylation. FR, flower removal. (**G**) Immunoprecipitation (Anti-Flag) showing that knockout of *SlLAX2* decreases SlARF2a SUMOylation. (**H** and **I**) Transient expression of *SlIAA3* (WT-SIM) or *SlIAA3* (SIM mutant) (H) or *SlIAA32* (WT-SIM) or *SlIAA32* (SIM mutant) (I) with *SlARF2a-Flag* or *SlARF2a-Flag* (3*K/R), followed by immunoprecipitation and immunoblot analysis revealing that SlIAA3 and SlIAA32 interact with SlARF2a in SIM- and SUMO-dependent manner. (**J** to **O**) Number of hours required for WT and *SlIAA3*-OE (J); WT and *SlIAA32*-OE (K); WT, *Sliaa3*, and *SlIAA3dIImSIMm*-OE *Sliaa3* (L); WT, *Sliaa32*, and *SlIAA32SIMm*-OE *Sliaa32* (M); WT, *Sliaa3*, and *Sliaa3 Slarf2a* (N); and WT, *Sliaa32*, and *Sliaa32 Slarf2a* (O) plants to achieve 50% abscission. dIIm, mutated domain II; SIMm, mutated SIM domain. Actin as the loading control. Significant differences were determined by one-way ANOVA with Dunnett's [(A), (E), (J), and (K)] and Tukey's [(L) and (M)] test; $^{**}P < 0.01$; $^{***}P < 0.001$; $^{****}P < 0.0001$; different lowercase letters indicate significant differences ($P < 0.05$). Boxplots show data from six independent tests, each consisting of at least 15 pedicels with maxima, first quartile, median, third quartile, and minima. h, hours.

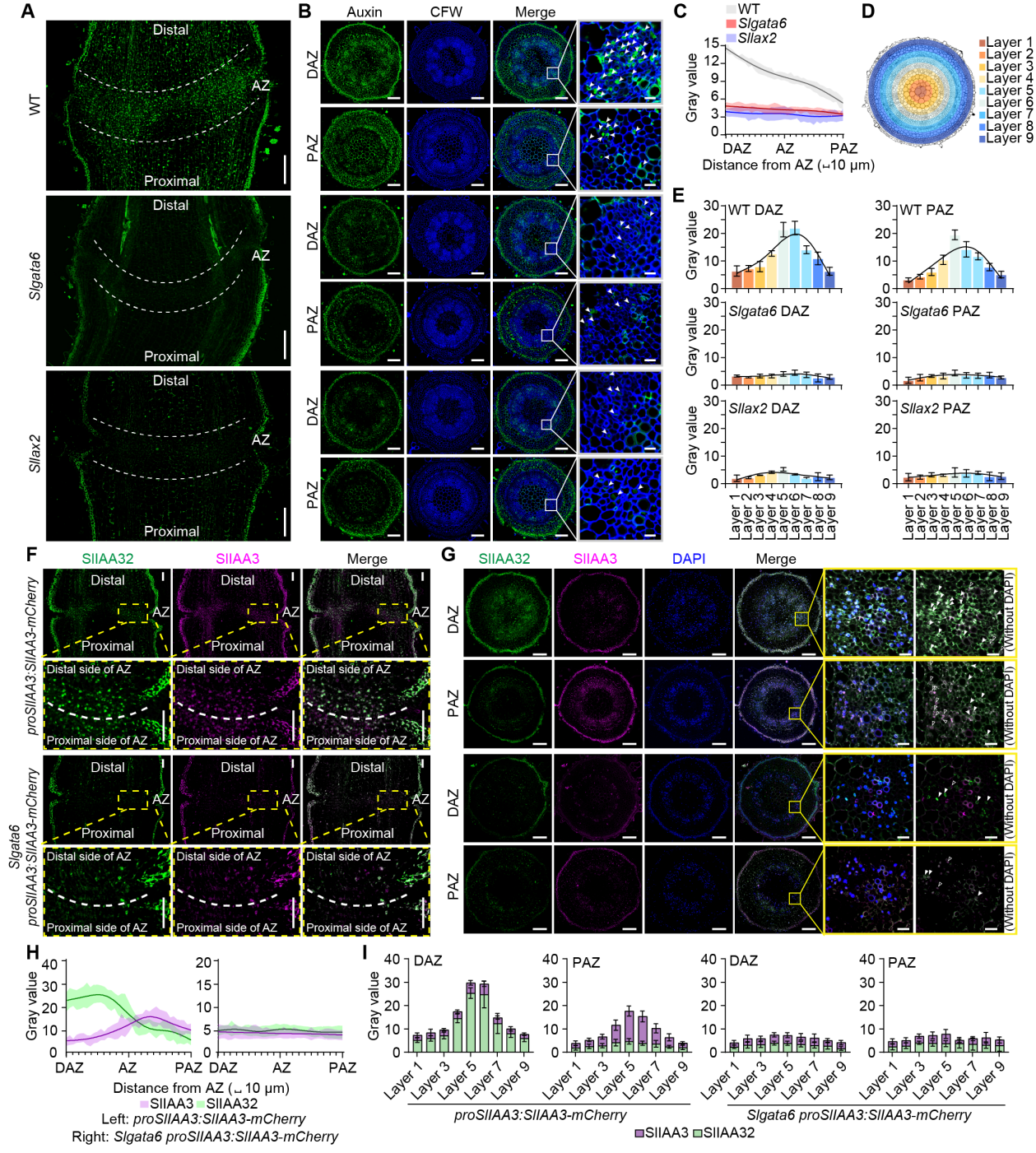

Fig. 5. SlGATA6 regulates the distribution of auxin, SlIAA3, and SlIAA32 throughout the AZ. (**A** and **B**) Immunolocalization of IAA in AZ of WT, *Slgata6*, and *Sllax2* plants. Longitudinal section view (A); transverse section view (B). Arrow indicates intracellular auxin. (**C**) Quantification of the fluorescence intensity in (A). (**D**) In transverse section view, we divided the area from pith to epidermis into nine layers for quantification. (**E**) Quantification of the fluorescence intensity in (B). (**F** and **G**) Immunolocalization of SlIAA32 and SlIAA3-mCherry in AZ of WT and *Slgata6* plants. Longitudinal section view (F); transverse section view (G). Solid triangles represent SlIAA32 protein, and hollow triangles represent SlIAA3 protein. Arrows indicate the presence of both SlIAA32 and SlIAA3 proteins. (**H** and **I**) Quantification of the fluorescence intensity in [(F) and (G)]. Scale bars, 200 μm [(A), (B), (F), and (G) complete view] and 20 μm [(B) and (G) magnified view]. Quantification of signal intensity from the distal side of the AZ (DAZ) to the proximal side of the AZ (PAZ) ($6 \leq n \leq 10$) was conducted using ImageJ [(C) and (H)]. Quantification of signal intensity at the distal side of the AZ (DAZ) and the proximal side of the AZ (PAZ) ($6 \leq n \leq 8$) was conducted using ImageJ [(E) and (I)]. Shades around lines depict 95% confidence interval [(C) and (H)].

with a similar phenotype observed in the knockout of *SlLAX2* (Fig. 5, A to E).

We generated *proSlIAA3:SlIAA3-mCherry* transgenic tomato plants and assessed SlIAA3 accumulation by using an antibody against mCherry. The mCherry signal was more abundant in the proximal side of the AZ compared to the distal part of the AZ, while knockdown of *SlIAA3* by VIGS led to a marked decrease of SlIAA3 accumulation in the proximal side of the AZ (fig. S13, A and B). We also investigated SlIAA3 and SlIAA32 distribution by double immunofluorescence labeling using monoclonal antibodies specifically recognizing mCherry or SlIAA32. In *proSlIAA3:SlIAA3-mCherry* plants, SlIAA32 highly accumulated in the distal side of the AZ, but not in the proximal side of the AZ, similar to the auxin distribution; we observed an opposite accumulation pattern for SlIAA3, with lower SlIAA3 accumulation in the distal side of the AZ than in the proximal side of the AZ (Fig. 5, F to I). These results suggest that the changes in auxin concentration and signaling in cells of different AZ regions control abscission.

We crossed *Slgata6* to the *proSlIAA3:SlIAA3-mCherry* line and measured SlIAA3 and SlIAA32 accumulation in the resulting *Slgata6 proSlIAA3:SlIAA3-mCherry* line by double immunofluorescence labeling. Knockout of *SlGATA6* abolished SlIAA3-mCherry and SlIAA32 accumulation across the AZ (Fig. 5, F to I), which was highly similar to the pattern seen following flower removal in *proSlIAA3:SlIAA3-mCherry* lines (4 hours after flower removal) (fig. S13, C to F). These results indicate that SlIAA3 and SlIAA32 distribution across the AZ is tightly regulated by SlGATA6.

SlARF2a functions downstream of SlGATA6-SlIAA3/SlLAX2 module to accelerate abscission

To further explore the relationship between SlLAX2 or SlIAA3 and SlGATA6 during abscission, we crossed *Sliaa3* to *Sllax2* to obtain *Sliaa3 Sllax2* double mutant lines, then crossed *Sliaa3*, *Sllax2*, and *Sliaa3 Sllax2* mutant lines to *SlGATA6*-OE plants. We observed that either single or double knockout of *SlIAA3* and *SlLAX2* in *SlGATA6*-OE plants significantly accelerated abscission compared with *SlGATA6*-OE plants, and there was no significant difference between the WT and *Sliaa3 Sllax2 SlGATA6-OE* plants (fig. S14A). We also crossed *Slgata6* to the *Slarf2a* mutant: The resulting *Slgata6 Slarf2a* double mutant line displayed a delayed abscission phenotype compared to that of *Slgata6* (fig. S14B). These results indicate that SlLAX2 and SlIAA3 function nonredundantly and act downstream of SlGATA6, while SlARF2a functions downstream of SlGATA6-SlIAA3/SlLAX2 module to modulate abscission.

SlKD1 induced abscission by repressing the function of SlGATA6

Our previous research indicated that *SlKD1* expression is up-regulated in abscission induced by flower removal (auxin gradient depletion) and under low-light conditions, promoting tomato pedicel abscission (*12*, *32*), and RT-qPCR assay further indicated that (fig. S15). Low light also induced *SlGATA6* expression (fig. S16A). However, in low light, *Slgata6* mutants showed more flower drop until fruit set, while fewer flowers dropped in *SlGATA6*-OE lines (Fig. 6A and fig. S16B). This finding indicates that SlGATA6 inhibits abscission.

To study the relationship between SlKD1 and SlGATA6, we crossed *SlKD1*-RNAi lines with *Slgata6* mutants and assessed the abscission phenotype of *Slgata6 SlKD1*-RNAi line. After auxin depletion imposed by flower removal, knocking out *SlGATA6* in the *SlKD1*-RNAi background suppressed the delayed abscission phenotype of the *SlKD1*-RNAi lines (Fig. 6B). Similarly, under low light, knockout of *SlGATA6* in the *SlKD1*-RNAi line resulted in more flower dropping compared to *SlKD1*-RNAi lines (Fig. 6C). We then examined plants knocked out for *SlLAX2* and/or *SlIAA3* in the *SlKD1*-RNAi background. After auxin depletion, *Slliaa3 SlKD1*-RNAi plants reached 50% abscission in 24.6 hours, while *Sllax2 SlKD1*-RNAi plants reached 50% abscission in 26.3 hours, and *Slliaa3 Sllax2 SlKD1*-RNAi plants reached 50% abscission in 16.2 hours (Fig. 6B). Low light induced 43.7% flower drop in *Sliaa3 SlKD1*-RNAi, 42.7% in *Sllax2 SlKD1*-RNAi, and 55.3% in *Sliaa3 Sllax2 SlKD1*-RNAi (Fig. 6C). This result indicates that SlKD1 induces abscission via SlGATA6.

Because SlKD1 interacts with the C-terminal ZnF domain of SlGATA6, and the ZnF domain is the DNA-binding domain, we conducted an EMSA to assess the influence of this interaction on the transcriptional activation activity of SlGATA6. EMSAs indicated that SlGATA6 can bind to the *SlIAA3* and *SlLAX2* promoters, while SlKD1 alone could not. When increasing amounts of recombinant SlKD1 were added, the binding of SlGATA6 to the *SlIAA3* and *SlLAX2* promoters was weaker; however, $SlKD1_{\Delta C}$ lacking the C terminus failed to impair the binding of SlGATA6 to the *SlIAA3* and *SlLAX2* promoters (Fig. 6D).

Next, we investigated whether the SlKD1-SlGATA interaction affected the binding of SlGATA6 to the *SlIAA3* and *SlLAX2* promoters in *N. benthamiana* leaves using a GUS transactivation assay. Coinfiltration of *35S:SlKD1* with *35S:SlGATA6* and *proSlIAA3:GUS* or *proSlLAX2:GUS* significantly inhibited the relative GUS activity induced by *35S:SlGATA6* alone, while coinfiltration of *35S:SlGATA6* with *35S:*$SlKD1_{\Delta C}$ and *proSlIAA3:GUS* or *proSlLAX2:GUS* did not affect GUS activity (Fig. 6E).

Then, we crossed *SlGATA6*-Flag-OE lines to *SlKD1*-RNAi (RNA interference) lines and performed chromatin immunoprecipitation–quantitative PCR (ChIP-qPCR) analysis to determine whether SlKD1 affects SlGATA6 binding to the *SlIAA3* and *SlLAX2* promoters in vivo. *SlGATA6*-Flag-OE and *SlGATA6*-Flag-OE *SlKD1*-RNAi plants showed no significant difference in terms of their SlGATA6 binding to the *SlIAA3* or *SlLAX2* promoters under normal conditions. However, *SlGATA6*-Flag-OE *SlKD1*-RNAi plants showed higher binding activities for SlGATA6 to the *SlIAA3* and *SlLAX2* promoters than *SlGATA6*-Flag-OE after flower removal and under low light (Fig. 6F). In agreement with this result, *SlIAA3* and *SlLAX2* expression levels were higher in *SlGATA6*-Flag-OE *SlKD1*-RNAi plants than in *SlGATA6*-Flag-OE plants under low-light and auxin depletion conditions (fig. S16C). All these results suggest that SlKD1 represses the transcriptional function of SlGATA6 to induce *SlLAX2* and *SlIAA3* transcription during abscission induced by auxin depletion brought upon by flower removal and low light.

As the KD1 shows less effect on GATA6 binding to the *SlIAA3* or *SlLAX2* promoters under normal conditions, we further explored the expression levels of *SlLAX2* and *SlIAA3* in *SlKD1*-OX plants and WT. The results indicated that *SlLAX2* and *SlIAA3* of *SlKD1*-OX plants were slightly low but not significant compared to those in WT (fig. S17). To further understand the impact of SlKD1 on the transcriptional regulation of SlGATA6, we first examined the detailed expression location of *SlGATA6* and *SlLAX2* in the AZ (Fig. 6G). A detailed localization of *SlGATA6* and *SlLAX2* transcript in specific cell layers in WT plants showed that *SlGATA6* level remained high in the distal side of AZ but was low on the proximal of AZ, *SlLAX2*

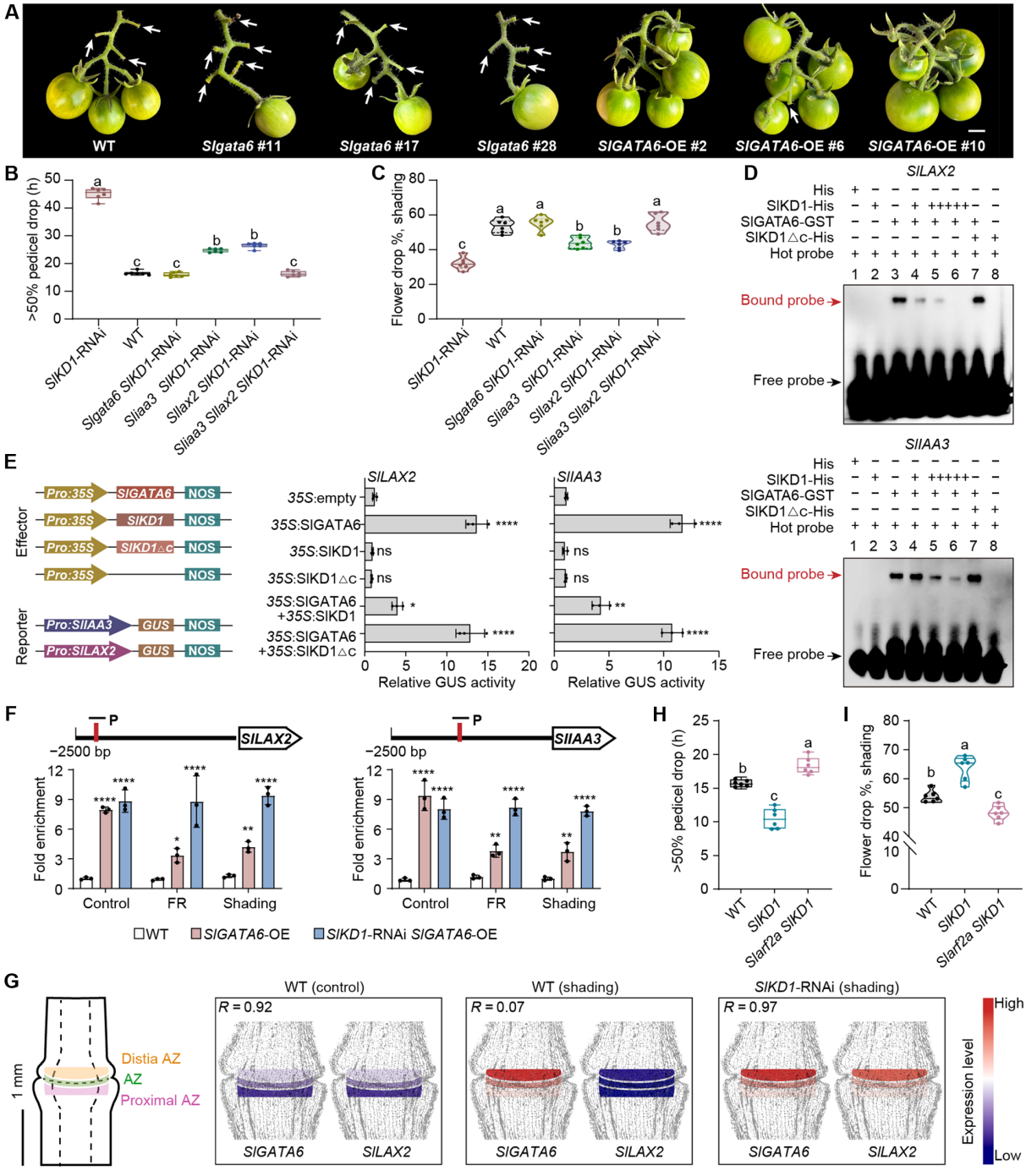

Fig. 6. Auxin depletion and low light induce SlKD1 to repress the SlGATA6-SlLAX2/SlIAA3 module to promote abscission. (**A**) Flower drop phenotypes of WT, *Slgata6*, and *SlGATA6*-OE plants. Arrows indicate AZ. Scale bar, 1 cm. Images were digitally extracted for comparison. (**B** and **C**) Number of hours needed for WT, *SlKD1*-RNAi, *Slgata6 SlKD1*-RNAi, *Sliaa3 SlKD1*-RNAi, *Sllax2 SlKD1*-RNAi, and *Sliaa3 Sllax2 SlKD1*-RNAi plants to achieve 50% abscission (B) and frequency of flower abscission (C). $n = 6$. (**D**) EMSA showing that SlKD1 does not bind to the *SlLAX2* and *SlIAA3* promoters but inhibits the binding of SlGATA6 to their promoters. (**E**) Promoter activity assay indicating that SlKID1, but not SlKD1$_{\Delta C}$, represses the transcriptional induction of *proSlLAX2:GUS* or *proSlIAA3:GUS* by SlGATA6. Values are means ± SD from three biological replicates. (**F**) Chromatin immunoprecipitation followed by quantitative PCR (ChIP-qPCR) analysis of SlGATA6-Flag enrichment at the *SlLAX2* and *SlIAA3* promoters in *SlGATA6*-OE and *SlGATA6*-OE *SlKD1*-RNAi lines following flower removal or shading treatment. Upper panel shows the localization of the PCR products tested for enrichment (top, black) and SlGATA6 binding sites (red). FR, flower removal. (**G**) Tomato pedicel AZ was divided into three zones using laser microdissection: distal AZ, AZ, and proximal AZ. Expression levels for each gene are represented according to a color scale. (**H** and **I**) Number of hours needed for WT, *SlKD1*-OX, and *Slarf2a SlKD1*-OX plants to achieve 50% abscission (H) and frequency of flower abscission (I). $n = 6$. One-way ANOVA with Tukey's test [(B), (C), (E), (H), and (I)] was used to assess statistical significance; $^*P < 0.05$, $^{**}P < 0.01$, $^{****}P < 0.0001$; different lowercase letters indicate significant differences ($P < 0.05$); ns, no significant difference. Boxplots and violin plots show maxima, first quartile, median, third quartile, and minima.

showed a similar phenotype under normal conditions, and the expression level of SlLAX2 is positively correlated with that of SlGATA6. However, under low-light conditions, the transcriptional level of *SlGATA6* shows an increase in the distal side of the AZ, while that of *SlLAX2* did not. The expression level of *SlLAX2* is not correlated with that of SlGATA6. After knockdown of *SlKD1*, under low-light conditions, the expression patterns of SlLAX2 and SlGATA6 became similar and exhibited a high positive correlation. Those results indicated that SlKD1 plays a minor role in regulating SlGATA6 activities under normal conditions, probably by posttranslation modified to regulate its unstable protein. Under low-light and flower removal conditions, the stable SlKD1 exerts an inhibitory effect on the function of SlGATA6.

Furthermore, we crossed *SlKD1*-OE lines to *Slarf2a* lines; after auxin depletion, knockout of *SlARF2a* in the *SlKD1*-OE background delayed the accelerated abscission of *SlKD1*-OE lines (Fig. 6H) and repressed the enhanced flower drop of *SlKD1*-OE under low-light conditions (Fig. 6I). These results suggest that the SlKD1-regulated SlGATA6-SlLAX2/SlIAA3 module is involved in auxin depletion– and low light–induced abscission.

The KD1-GATA6 module is conserved in Solanaceae during abscission

Compared to other tomato *TKN* homologs, the KNOX2 domain in SlKD1 appears to be unique (Fig. 7A). SlGATA6 failed to interact with other members of the KONX family genes that contain the KNOX2 domain in Y2H assay (fig. S18), suggesting that SlKD1 plays a unique role in mediating tomato pedicel abscission. Moreover, we discovered that the KNOX2 domain of SlKD1 is highly conserved in the other Solanaceae species potato (*Solanum tuberosum*), eggplant (*Solanum melongena*), and pepper (*Capsicum annuum*) (Fig. 7B). In addition, all of these species have a protein related to SlGATA6 with a similar ZnF domain (Fig. 7C). Shading can also cause flower drop in potato, eggplant, and pepper plants (Fig. 7, D, G, and J). Thus, we asked whether the KD1-GATA module might be conserved in the shading-induced flower abscission of Solanaceae species. To verify this assumption, we used VIGS to knock down *KD1* or *GATA6* in potato, eggplant, and pepper and measured the flower abscission rate under low-light conditions (Fig. 7). The knockdown of each *KD1* ortholog resulted in decreased flower drop under shading, while the knockdown of each *GATA6* ortholog led to the opposite phenotype. Thus, the KD1-GATA6 module is conserved in these three Solanaceae crops. Together, our data indicate that flower abscission may be regulated by the KD1-GATA6 module, which is deeply conserved in Solanaceae species.

DISCUSSION

Local auxin-response gradient in AZ is necessary for inhibiting abscission. Destruction of auxin-response gradient induces abscission, and a complex network that involves multiple auxin-related genes spatially and temporally regulates this process. Here, we report the role and regulatory mechanism of low light and auxin depletion on interrupting the auxin-response gradient and inducing abscission.

The immunofluorescence results show that there are more cells holding high auxin at the distal side of the AZ than at the proximal side (Fig. 5). This difference causes a higher concentration of auxin at the distal end than the proximal end, resulting in an auxin gradient across the AZ. SlLAX2 is the key to the formation of this auxin gradient, which is important for maintaining auxin-response gradient and preventing abscission in two aspects. First, SlARF2a plays a major role in depressing the auxin-response and positively regulating ethylene response; hence, it was identified as a vital abscission inducer (Fig. 4 and fig. S11G). The auxin-dependent SUMOylation site within SlARF2a is vital for inhibiting its function. Second, the high concentration of auxin that depends on SlLAX2 promotes the stability of the noncanonical Aux/IAA, SlIAA32, which maintains the auxin-response gradient and prevents abscission by interacting with SlARF2a in a SlLAX2-dependent SUMOylation manner (Fig. 4 and fig. S11H). Moreover, we found that *SlIAA3* was highly expressed in the AZ and preferentially accumulated in the proximal region of the AZ, where the auxin concentration is relatively low (Fig. 5). We also revealed that SlIAA3 maintains the auxin-response gradient and represses abscission by interacting with and repressing the SUMOylation of SlARF2a, thereby inhibiting its function (Fig. 4, H, J and L). Considering that SlIAA3 is a canonical Aux/IAA and is degraded in an auxin-dependent pathway, the stability of the noncanonical Aux/IAA SlIAA32 increased as the auxin concentration increased, and both of them contribute to repress the function of SlARF2a. We reasonably deduced that the high auxin concentration of the AZ cell promotes auxin response mainly through SlIAA32, with little contribution from SlIAA3. The middle auxin level in the AZ may exert its function through the combined action of SlIAA32 and SlIAA3, while the low auxin concentration functions through SlIAA3 alone. Although SlIAA32 and SlIAA3 exhibit opposite distribution patterns across the AZ, the combined signal of these two auxin-response enhancers is higher on the distal side than on the proximal side. We suggested that the cells in the distal side of AZ mainly rely on SlIAA32 and slightly rely on SlIAA3 to maintain a high auxin response. Meanwhile, the cells in the AZ use both SlIAA32 and SlIAA3 to maintain a moderate auxin response, and the cells in the proximal side of the AZ mainly depend on SlIAA3 and a small amount of SlIAA32 to form a relatively low auxin response (Fig. 8A).

The DAP-seq indicated that SlGATA6 promotes *SlLAX2* and *SlIAA3* expression by directly binding to a "GATC" motif in the *SlLAX2* and *SlIAA3* promoters (Fig. 2). Genetic evidence indicates that SlLAX2 and SlIAA3 act downstream of GATA6 and play nonredundant roles in inhibiting abscission. We found that SlGATA6 does not directly bind to the promoter of SlIAA32. Using the Plant Care (http://bioinformatics.psb.ugent.be/webtools/plantcare/html/) to explore the possible upstream regulators of SlIAA32, we identified several light-responsive elements, including G-Box, Box 4, Box II, GT1-motif, and TCCC-motif, and drought-responsive elements (MBS). Combined with SlIAA3 that functions downstream of SlGATA6 and participates in abscission induced by auxin depletion and low light, in contrast, SlIAA32 is potentially engaged in responses to light and drought. It is also reasonably deduced that having both SIAA3 and SIIAA32 could be important in a different way; these proteins, which work at different levels of auxin concentration, can provide a robust repression of SIARF2a during the fluctuation of auxin flow, which may be affected by environmental conditions.

Multiple studies indicate that environmental stresses or auxin depletion induce abscission, which requires an interruption of the auxin-response gradient (*9*, *12*, *46*, *47*). *SlKD1* transcript levels increase under auxin depletion and low-light conditions to induce abscission (*12*, *32*). SlKD1 physically interacts with SlGATA6 and

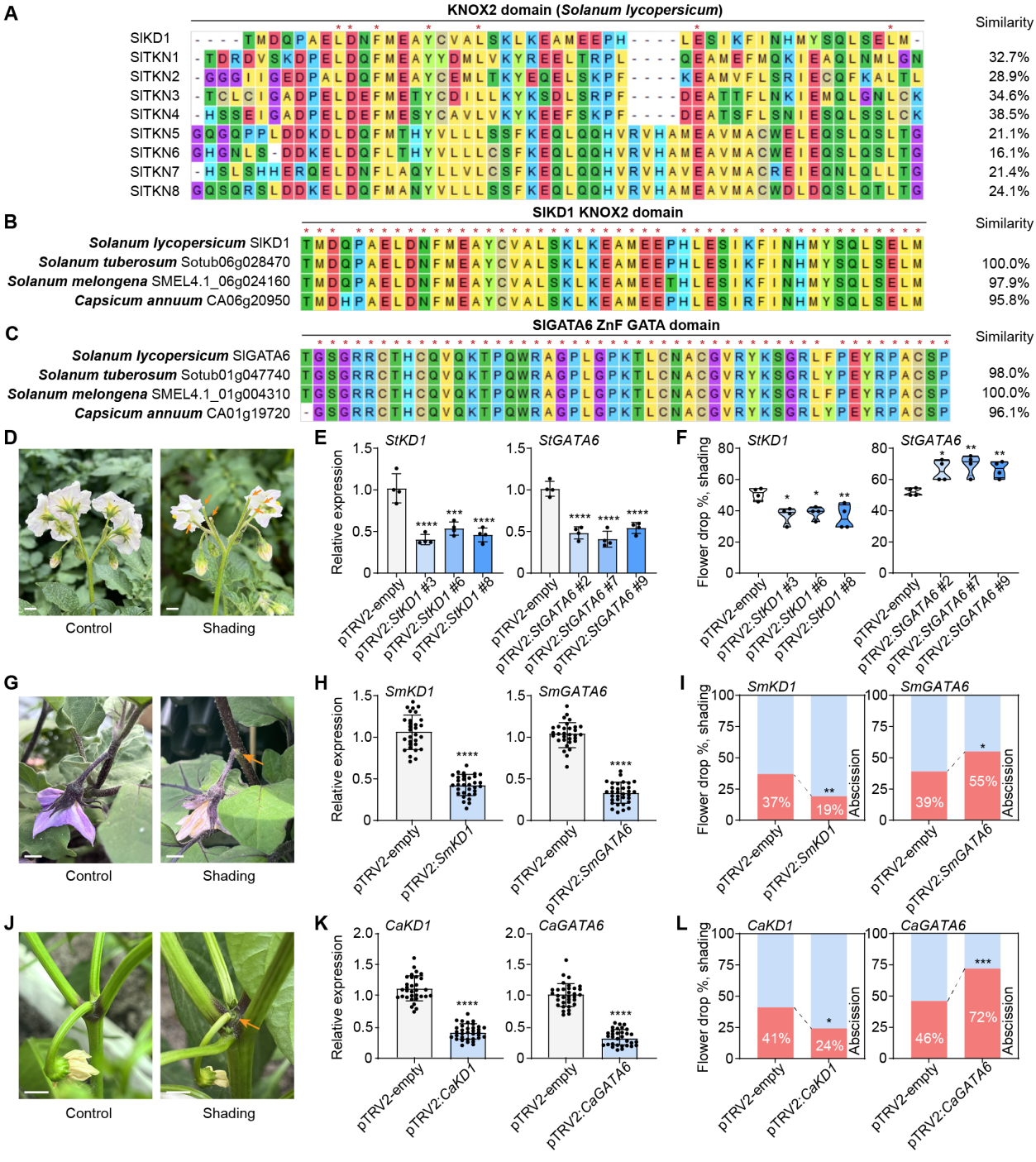

Fig. 7. The KD1-GATA6 module is conserved in three Solanaceae crops. (**A**) Alignment of the KNOX2 domain from SlKD1 and other SlTKN proteins. (**B**) Alignment of the tomato KD1-KNOX2 domain of SlKID1 with that from the orthologs of other Solanaceae crops. (**C**) Alignment of the GATA6-ZnF GATA domain from SlGATA6 with that from the orthologs of other Solanaceae crops. (**D**) Potato flower abscission phenotype under low light. The orange arrows indicate the AZ. Scale bars, 1 cm. (**E**) Silencing efficiency of *StKD1* and *StGATA6* in their respective VIGS plants as determined by RT-qPCR. Values are means ± SD from four biological replicates. (**F**) Frequency of flower abscission in the pTRV2-empty, pTRV2:*StKD1*, and pTRV2:*StGATA6* plants under shading. Boxplots show data from four independent tests, each consisting of 10 to 14 flowers. Violin plot shows maxima, first quartile, median, third quartile, and minima. (**G**) Eggplant flower abscission phenotype under low light. The orange arrow indicates the AZ. Scale bars, 1 cm. (**H**) Silencing efficiency of *SmKD1* and *SmGATA6* in their respective VIGS plants as determined by RT-qPCR. (**I**) Frequency of flower abscission in the pTRV2-empty, pTRV2:*SmKD1*, and pTRV2:*SmGATA6* plants under shading. $n = 30$ to 35. (**J**) Pepper flower abscission phenotype under low light. The orange arrow indicates the AZ. Scale bars, 1 cm. (**K**) Silencing efficiency of *CaKD1* and *CaGATA6* in their respective VIGS plants as determined by RT-qPCR. (**L**) Frequency of flower abscission in the pTRV2-empty, pTRV2:*CaKD1*, and pTRV2:*CaGATA6* plants under shading. $n = 30$ to 35. One-way ANOVA with Dunnett's test [(E) and (F)], two-tailed Student's *t* test [(H) and (K)], and Fisher's exact test [(I) and (L)] was used to assess statistical significance; $^*P < 0.05$, $^{**}P < 0.01$, $^{***}P < 0.001$, $^{****}P < 0.0001$. Violin plots show maxima, first quartile, median, third quartile, and minima.

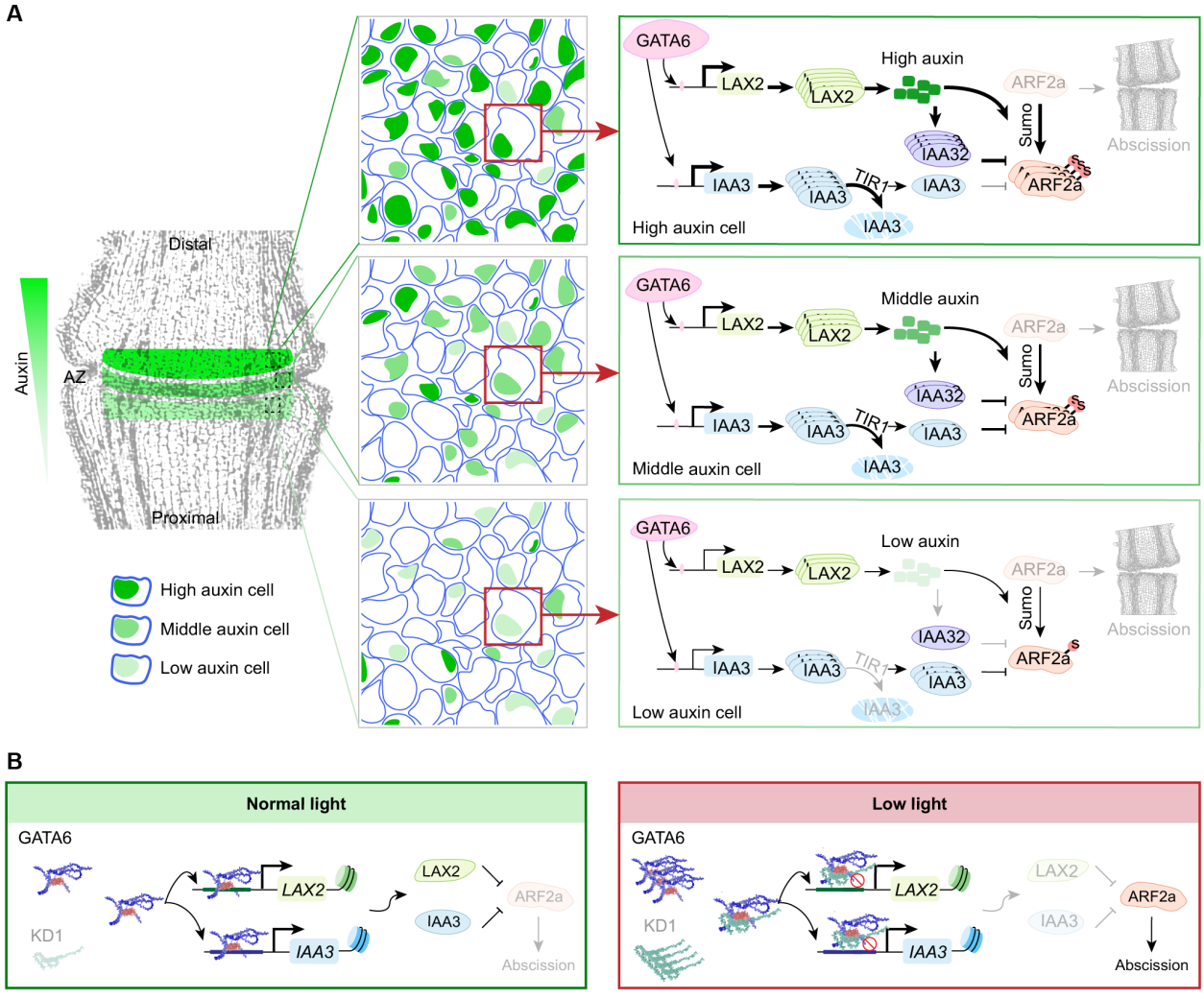

Fig. 8. Schematic model of how the GATA6-LAX2/IAA3 module inhibits abscission. (**A**) GATA6-LAX2/IAA3 module established auxin-response gradient across AZ. (**B**) Model of low light–induced modulation of tomato flower pedicel abscission by KD1-GATA6.

the interactions between them occurred between the C terminus of SlKD1 containing the KNOX2 domain and the C-terminal ZnF domain of SlGATA6. SlKD1 could not bind to the promoters of *SlLAX2* or *SlIAA3* on its own, but coexpression of *SlKD1* and *SlGATA6* suppressed the binding of SlGATA6 to the *SlLAX2* and *SlIAA3* promoters, as indicated by EMSAs and ChIP-PCR (Fig. 6). Knockdown of *SlKD1* delayed pedicel abscission induced by auxin depletion and the flower drop induced by low light, while knockout of *SlGATA6* abolished the lower abscission rate and flower drop defects seen in the *SlKD1*-RNAi line. We observed a similar abscission phenotype in *Sliaa3 SlKD1*-RNAi, *Sllax2 SlKD1*-RNAi, and *Sliaa3 Sllax2 SlKD1*-RNAi lines. Moreover, knockout of *SlARF2a* significantly slowed down the abscission rate of *SlKD1*-OE (Fig. 6). These results indicate that auxin depletion and low light induce pedicel abscission and flower drop by inducing *SlKD1* to repress the SlGATA6-SlIAA3/SlLAX2 module. However, this inhibition is obvious under low-light and auxin depletion conditions, but not under normal conditions. The regulation mechanism of low light and flower removal on posttranslation modification of SlKD1 needs to be studied in future works.

The KNOX2 domain of KD1 and the C-terminal ZnF domain of GATA6 are conserved among solanaceous species. Solanaceous family yields are typically lost in low-light conditions. Our research has demonstrated that the KD1-GATA6 module helped in inducing flower abscission in solanaceous species under low-light conditions. Our study provides KD1 as a potential target for inhibiting abscission and enhancing the yields of solanaceous crops under low-light conditions through gene editing technology.

In this study, we revealed that low light–induced *SlKD1* expression repressed the function of the SlGATA6-SlIAA3/SlLAX2 module to induce abscission, uncovering a regulatory mechanism by which low light mediates GATA function (Fig. 8B). Under normal conditions, the SlGATA6-SlIAA3/SlLAX2 module maintains the auxin-response gradient across the AZ to prevent abscission. Auxin depletion and low light promotes *SlKD1* transcription, which downregulates *SlLAX2* and *SlIAA3* expression, thus initiating abscission.

MATERIALS AND METHODS

Plant materials and growth conditions

The tomato (*S. lycopersicum*) cultivar "Ailsa Craig" was used as the WT in this study. Our laboratory was responsible for maintaining seeds for the *SlKD1*-OX, *SlKD1*-RNAi, and *DR5:GUS* transgenic tomato lines (*12*). Cultivated potato (*S. tuberosum*), eggplant (*S. melongena*), and pepper (*C. annuum*) were used for VIGS. Tomato, potato, eggplant, and pepper plants were cultivated in a controlled greenhouse environment, maintaining a temperature of 25°C for 16 hours during the day, followed by a temperature of 15°C for 8 hours at night. The experimental procedure for shading treatment and inducing fruit drop was conducted in accordance with a previously outlined methodology (*11*, *12*). The photosynthetically active radiation levels under normal light and low light were 600 and 180 μmol m^{-2} s^{-1}, respectively. *N. benthamiana* plants were used for biochemical experiments and grown under a 25°/18°C (day/night) temperature regime with a relative humidity of 60%.

Plasmid construction and tomato transformation

Transgenic tomato plants were generated using AC as the background. The CRISPR-Cas9 vectors were composed of the *Cas9* endonuclease gene and two single guide RNAs (sgRNAs), as detailed in the study conducted by Mao *et al.* (*48*). Two target sequences per gene of interest, sgRNA1 and sgRNA2, were designed based on target sites in the exons of *SlGATA6*, *SlLAX2*, *SlIAA3*, *SlIAA32*, and *SlARF2a* (see data S7). To conduct phenotypic tests, T2 homozygous lines lacking the *Cas9* transgene were identified by sequencing PCR products generated from the appropriate target areas. The primers used in this study are listed in data S7.

The pTA7002-*SlIAA3dIIm*, pTA7002-*SlIAA3dIImSIMm*, and pTA7002-*SlIAA32SIMm* constructs were generated by cloning the synthesized coding sequence encoding a domain II mutant of SlIAA3 or the SIM domain of SlIAA3/SlIAA32 into the pTA7002 vector, which had been digested with the restriction enzymes Xho I and Spe I. The full-length coding sequence of *SlIAA32* was also cloned by PCR and introduced into the pTA7002 vector. All resulting plasmids were introduced individually into Agrobacterium (*Agrobacterium tumefaciens*) strain LBA4404 via electroporation. The presence of the construct in each plant was assessed by PCR, using primers specifically designed to target the hygromycin resistance gene. Gene expression levels in transgenic plants were analyzed following treatment with a 1 mg/liter dexamethasone solution. Three T2 lines with the highest expression levels were chosen for phenotypic analysis and experiments.

The *SlGATA6*-OE, *SlLAX2*-OE, and *SlARF2a*-OE plants were generated by cloning the full-length coding sequence of *SlGATA6*, *SlLAX2*, and *SlARF2a* individually in pCAMBIA1300-Flag vectors. *SlARF2a*-$OE^{3*\ K/R}$ plants were generated by cloning the synthesized coding sequence of $SlIARF2a^{3*\ K/R}$ into the pCAMBIA1300-Flag vector, which had been digested with the restriction enzymes Eco RI and Bam HI. The *proSlIAA3:SlIAA3*-mCherry plants were generated by cloning a 2000-bp promoter fragment and full-length coding sequence of *SlIAA3* in the p2301-mCherry vector. The resulting constructs were introduced into Agrobacterium (strain LBA4404). Each construct was transformed into tomato (AC cultivar) using the leaf disc cocultivation method (*12*). Specific primers were used to detect *SlGATA6*, *SlLAX2*, and *SlARF2a* expression in transgenic plants, respectively. All primers used in this study are listed in data S7.

Moreover, on the basis of the morphological and histological data of mutant and transgenic plants, we discovered that, in comparison with WT plants, all the mutant/transgenic plants developed normal AZs. The differences in abscission between them and the WT were exhibited in the varying lengths of time necessary for the abscission (fig. S19).

Pedicel abscission assays

The experiments looking at flower pedicel abscission were conducted according to the methodology outlined in previous studies (*12*, *49*). In short, to analyze flower pedicel abscission rate, we used at least 15 flowers for each experiment. Flowers were manually removed (to eliminate the source of auxin and then promotes abscission), and flower pedicels were placed in 1% agar media for incubation. The time of flower removal was recorded as 0 hours and the number of flower pedicel abscission at various time intervals was then calculated as a percentage of the overall number. For 50% pedicel drop, a nonlinear fit was performed using Origin software, and the time required to achieve 50% abscission was computed.

The tomato was treated with low light before flowering, and the treatment was continued until the fruit was set. The percentage of flower drop for WT and mutant plants was calculated under normal and low-light conditions. We measured 20 to 30 flowers in four inflorescences in each experiment.

Virus-induced gene silencing

The VIGS experiments were mainly carried out as described in previous research (*50*). The VIGS tool available on the Sol Genomics Network (https://solgenomics.net/) website was used to design the specific fragments for knocking down *SlLAX2*, *SlIAA3*, *SlIAA11*, *SlIAA13*, *SlARF2a*, *SlARF4*, *SlARF6*, *SlARF14*, *StKD1*, *StGATA6*, *SmKD1*, *SmGATA6*, *CaKD1*, and *CaGATA6*. Each fragment was amplified through PCR and then inserted into the pTRV2 vector. The resulting constructs, the pTRV2 empty vector, and the pTRV1 vector were separately introduced into Agrobacterium strain GV3101. As previously described (*51*–*54*), Agrobacterium cultures harboring pTRV1 or pTRV2 or each pTRV2 derivative were suspended using buffer (10 mM MES, 10 mM $MgCl_2$, and 200 mM acetosyringone, pH 5.6) and mixed in a 1:1 (v/v) ratio before infiltrating the stem of tomato, potato, eggplant, or pepper plants. The silencing efficiency was assessed by RT-qPCR at the time of flower blooming. The primers are listed in data S7.

RNA extraction and RT-qPCR analysis

The AZs of various plants were collected and frozen in liquid nitrogen and preserved at −80°C. An RNA Pure Plant Kit (CWBIO, Cambridge, MA, USA) was used to extract total RNA from samples. One microgram of total RNA was converted into first-strand cDNA using a PrimeScript 1st strand cDNA Synthesis Kit (Takara). qPCR was performed using SYBR Premix (Takara) on a qTOWER3/G real-time instrument (Analytik Jena). *SlACTIN*, *StEF1-α*, *SmACTIN*, and *CaACTIN* genes were used as internal controls for their respective plant species. Relative gene expression levels were calculated using the $2^{-\Delta\Delta Ct}$ method (*55*). Detailed qPCR primer sequences are listed in data S7.

Sequence alignment and phylogenetic analysis

The amino acid sequences of the KNOX2 domain from KNT in tomato and the KNOX2 domain and ZnF-GATA6 domains from potato, eggplant, and pepper proteins were obtained from the Sol Genomics Network (https://solgenomics.net/) website by BLAST

search. The multiple sequence alignment was conducted using MEGA7 software. Phylogenetic analysis using the amino acid sequences for the tomato and *Arabidopsis* GATA proteins was performed using MEGA7 software with the neighbor-joining method with a bootstrap test of 1000 replicates.

Y2H assay

A cDNA library was constructed from mRNA extracted from flower AZs harvested at 0, 2, 4, 8, 12, and 16 hours following abscission induced by auxin depletion (flower removal) using the Make Your Own Mate & Plate Library System (Clontech, http://clontech.com/). The full-length coding sequence of *SlKD1* was introduced into the pGBKT7 vector; the resulting construct was used as bait. The above library was screened using a Yeastmaker Yeast Transformation System 2 kit (Clontech, 630439).

The sequences encoding the fragments $SlKD1_N$ (amino acids 1 to 79) and $SlKD1_C$ (amino acids 80 to 171) were individually cloned into the pGBKT7 vector. The sequences encoding the fragments KNOX2 domain of *SlTKN1* to *SlTKN18* were individually cloned into the pGBKT7 vector. The full-length coding sequence of *SlGATA6*, $SlGATA6_N$ (encoding amino acids 1 to 157 of SlGATA6), $SlGATA6_M$ (encoding amino acids 158 to 233 of SlGATA6), and $SlGATA6_C$ (encoding amino acids 234 to 325 of SlGATA6) sequences were cloned into the pGADT7 vector. All primers used in this study are listed in data S7. The resulting pGBKT7 and pGADT7 constructs were cotransformed as appropriate pairs into the yeast strain Y2H-Gold. The transformants were plated on synthetic defined medium lacking Leu and Trp and allowed to grow at 30°C for 3 to 5 days. Positive transformants were spotted onto synthetic defined medium lacking Leu, Trp, His, and Ade and containing Aureobasidin A (AbA; 150 ng/ml) and allowed to grow at 30°C for 3 to 5 days. The combination of BD-53 and AD-T was used as a positive control, and the combination of BD-Lam and AD-T was used as a negative control.

Protein extraction and immunoblotting

Total protein from tomato pedicel AZ or *N. benthamiana* leaves was extracted using radioimmunoprecipitation assay buffer (Solarbio, R0010). Immunoblot analysis was performed using the Magnetic IP/Co-IP Kit (Thermo Fisher Scientific, 88804). The antibodies used were as follows: anti-GST (1:8000 dilution; Solarbio, K200006M), anti-His (1:3000 dilution; Solarbio, K200060M), anti-GFP (1:3000 dilution; Solarbio, K114305P), anti-Flag (1:5000 dilution; CST, #14793), anti-Actin (1:2000 dilution; Biopm, PMK085S), anti-HA (1:3000 dilution; Solarbio, K007440P), anti-MYC (1:3000 dilution; Solarbio, K106458P), anti-SUMO1 (1:1000 dilution; Abcam, ab5316), and anti-SlIAA32 (SSEYLLNHATTLPSVYY; 1:1000 dilution; synthesized by Abmart Shanghai Co. Ltd. synthesis). The secondary antibodies used were goat anti-rabbit IgG (H + L)–horseradish peroxidase conjugate (1:30,000 dilution; EASYBIO, BE0101) and goat anti-mouse IgG (H + L)–horseradish peroxidase conjugate (1:3000 dilution; Bio-Rad, 170-6516). The membranes were incubated with ECL chemiluminescent substrate (Super sensitive) (Biosharp, BL523) before the signals were captured on an Azure Biosystems C600 (America).

Pull-down assay

The full-length or C-terminal coding sequences of *SlKD1* and *SlGATA6* were individually amplified by PCR from WT cDNA and cloned into pET30a and pGEX-6P-1, respectively. Primer sequences are listed in data S7. The plasmids were then individually transformed into *Escherichia coli* strain BL21. One positive colony per construct was grown at 37°C until the OD_{600} (optical density at 600 nm) reached 0.6 to 0.8. Protein production was induced for 16 hours at 18°C by the addition of 0.25 mM isopropyl-β-D-thiogalactopyranoside (IPTG). Recombinant SlKD1-His or SlKD1c-His was purified using Ni-NTA agarose (Beyotime, P2241). Recombinant SlGATA6-GST, SlGATA6c-GST, or GST (negative control) was incubated with GST beads (Beyotime, P2262-1). SlKD1-His or SlKD1c-His was added to the GST beads covered with SlGATA6-GST, SlGATA6c-GST, or GST. After incubation at 4°C for 1 hour, the beads were washed three times with phosphate-buffered saline (PBS, pH 7.2 to 7.4). The bound proteins were then eluted with elution buffer (10 mM GSH, 8 mM Na_2HPO_4, 136 mM NaCl, 2 mM KH_2PO_4, and 2.6 mM KCl). The eluted proteins were detected by immunoblotting as above.

Immunoprecipitation assay

Total protein from tomato pedicel AZ from *SlARF2a-Flag* OE, $SlARF2a^{3*K/R}$*-Flag* OE, and *Sllax2 SlARF2a-Flag* OE plants was extracted with lysis buffer (Beyotime, P0043), to which the protease inhibitor phenylmethylsulfonyl fluoride (PMSF) was added (1 mM, Beyotime, ST506-2). The mixture was subjected to high-speed centrifugation at 14,000*g* for 15 min at 4°C. To the resulting supernatant, 50 μl of anti-Flag beads (Beyotime, P2115) was added, followed by incubation on ice for 2 hours. The beads were collected by magnetic separation rack and then washed three times with 1 ml of cold lysis buffer each time. After the final wash, 100 μl of preheated (95°C) 1× SDS-loading buffer was added to the beads to elute the immunocomplex. The immunoprecipitated proteins were examined by immunoblotting using anti-Flag and anti-SUMO1 antibodies.

Co-IP assay

Transient expression in *N. benthamiana* leaves was used for co-IP. The full-length coding sequences of *SlKD1* and *SlGATA6* were individually amplified from AC cDNA and cloned into the pCAMBIA1300-Flag vector and pCAMBIA1300-GFP vector, respectively. For the construction of *SUMO-HA*, *SlARF2a-Flag*, *SlIAA3-MYC*, and *SlIAA32-MYC* constructs, the full-length coding sequences of *SUMO*, *SlARF2a*, *SlIAA3*, and *SlIAA32* were individually amplified from WT cDNA using specific primers and introduced into the pRI101-AN vector with the appropriate tag (*56*). Primers used for vector construction are listed in data S7. The resulting plasmids were individually transformed into Agrobacterium strain GV3101 for infiltration of *N. benthamiana* leaves. After 2 days, leaves were collected and homogenized in lysis buffer (with PMSF) at 4°C for 30 min. The mixture was subjected to high-speed centrifugation at 14,000*g* for 15 min at 4°C. The resulting supernatant was incubated with 50 μl of anti-GFP beads (Beyotime, P2132) or anti-Flag beads (Beyotime, P2115) for 2 hours at 4°C. Subsequent steps were as described above for immunoprecipitation. Proteins were probed by immunoblotting with anti-GFP, anti-Flag, anti-MYC, and anti-HA antibodies.

Subcellular localization and BiFC assays

For subcellular localization, the full-length coding sequence of *SlGATA6* was amplified by PCR from WT cDNA and cloned into the pCAMBIA1300-GFP vector. For BiFC, the full-length coding sequence of *SlKD1* and a fragment encoding $SlKD1_C$ or $SlKD1_{\Delta C}$ were cloned in the pCAMBIA1300-nYFP vector; the full-length coding sequence of *SlGATA6* and a fragment encoding $SlGATA6_C$ or $SlGATA6_{\Delta C}$ were cloned in the pCAMBIA1300-nYFP vector. The

primers used for vector construction are described in data S7. The resulting plasmids were individually transformed into Agrobacterium strain GV3101 for infiltration of *N. benthamiana* leaves. Protoplasts were created 3 days after infiltration by immersing converted leaves in the Plant Protoplasts Isolation Kit (Beyotime, C0362S) and gently agitating for 1 hour in the dark. The protoplast suspensions were centrifuged at 200*g* for 1 min. The supernatant was discarded, and the pellet was gently resuspended in the remaining supernatant. Fluorescence in *N. benthamiana* leaves was captured at 3 days after infiltration using a Leica TCS SP8 81-1557 confocal laser scanning microscope. Excitation/emission wavelengths were 488 nm/506 to 538 nm for YFP and GFP, respectively. NF-YA4-mCherry and 4′,6-diamidino-2-phenylindole (DAPI, Beyotime, C1002) were used as nuclear localization markers, with excitation/emission wavelengths of 359 nm/457 nm (mCherry) and 587 nm/610 nm (DAPI).

RNA in situ hybridization

RNA in situ hybridization was conducted as outlined in a recent study by Wang *et al.* (*57*). In brief, a specific fragment of the coding sequence of *SlGATA6*, *SlLAX2*, *SlIAA3*, *SlIAA32*, and *SlARF2a* was amplified and subsequently inserted into the pSPT18 and pSPT19 vectors (Roche, Basel, Switzerland). The antisense and sense RNA probes were synthesized using SP6 and T7 RNA polymerase, respectively, following the established methodology outlined in the DIG Oligonucleotide 3′-End Labeling Kit (Roche). Probe information is given in data S7.

RNA-seq analysis

TRIzol Reagent (Invitrogen, 15596026) was used to extract total RNA from the AZ of AC and *SlGATA6* knockout transgenic plants, using two biological replicates. The concentration and purity of total RNA were assessed using a 2100 Bioanalyzer (Agilent). Two micrograms of total RNA was used for library construction using a KC Stranded mRNA Library Prep Kit for Illumina (catalog no. DR08402, Wuhan Seqhealth Co. Ltd., China). Products corresponding to 200 to 500 bp were purified, quantified, and eventually sequenced using a DNBSEQ-T7 sequencer (MGI Tech Co. Ltd., China) as 150-bp paired-end reads. The generation and sequencing of the libraries were conducted by Wuhan Kangce Technology Co. Ltd. (Wuhan, China). Using Trimmomatic (version 0.36), the raw sequencing data were filtered, and the clean reads were mapped to the tomato reference genome (version: SL4.0) using STRA software (version 2.5.3a) with default parameters. The analysis of DEGs was conducted using the edgeR package (version 3.12.1). The DEGs were filtered based on an absolute $\log_2$ fold change of at least 1 and an FDR below 0.01. KEGG pathway enrichment analysis was implemented using KOBAS software (version 2.1.1). The validity of the RNA-seq data was verified through RT-qPCR on a randomly selected gene. The sequences of primers can be found in data S7.

DAP-seq and data analysis

DAP-seq was carried out according to a previously published method (*12*). The full-length coding sequence of *SlGATA6* was cloned into the pET15b-Halo vector, carrying a sequence encoding the Halo tag. A genomic DNA library was prepared from tomato AZs following the guidelines provided by the manufacturer (Illumina). Recombinant SlGATA6-Hola protein was purified and the DNA targets were enriched, followed by sequencing on an Illumina HiSeq 4000 instrument (Gene Denovo Biotechnology Co., China). The clean reads were aligned to the tomato reference genome (version SL4.0) using the Bowtie2 program (version 2.2.5). The binding peaks of SlGATA6 were identified using MACS2 software (version 2.1.2). The MEME suite (http://meme-suite.org/) was used to detect motifs.

Electrophoretic mobility shift assays

The full-length coding sequence of *SlGATA6* was cloned into the pGEX-6P-1 vector; the resulting plasmid was transformed into *E. coli* Rosetta cells. One positive colony was grown at 37°C until the OD_{600} reached 0.6 to 0.8. Protein production was induced for 16 hours at 18°C by the addition of 0.25 mM IPTG. Recombinant SlGATA6-GST was purified using a GST-Tag Protein Purification Kit (Beyotime, P2260S). Parts of promoter sequences of *SlLAX2*, *SlIAA3*, *SlIAA11*, and *SlIAA13*, tagged with biotin, are depicted in data S7. The 5′ biotin-labeled probe was synthetized by Saibaisheng Company (China). A nonlabeled probe was used as a competitor, while the labeled mutant probe served as a negative control. EMSA was performed using a Chemiluminescent EMSA Kit (Beyotime).

GUS staining and activity assay

GUS staining and activity assays were carried out according to published methods (*58*). For GUS staining, flower pedicels were incubated in GUS staining solution (Real-Times Biotechnology Co. Beijing, China) at 37°C for 24 hours in the dark. Three distinct plants were chosen for each genotype, from which at least 20 flower pedicels were collected. For GUS activity assays, the full-length coding sequence of *SlGATA6* and *SlKD1* and fragments of the *SlKD1* coding sequence ($SlKD1_{\Delta C}$) were individually cloned into the binary pRI101 vector. A 2200-bp promoter fragment for *SlLAX2*, *SlIAA3*, *SlIAA11*, and *SlIAA13* was cloned in the pBI101 vector upstream of the *GUS* reporter gene. The resulting plasmids were individually introduced into Agrobacterium strain EHA105 for infiltration of *N. benthamiana* leaves as described above. GUS activity was measured as previously described (*58*) with three biological replicates. The primers can be found in data S7.

Determination of auxin concentration

The content of IAA was measured as previously described (*58*). In brief, the IAA content was determined using LC-MS/MS analysis. The AZ segments of at least 40 flower pedicels were frozen and ground in liquid nitrogen, and then freeze dried in a vacuum oven set at −80°C. From each plant, 50 mg of powder was dissolved in 1 ml of a solution made of formic acid, water, and methanol (15:4:1, v/v/v). To each sample, 10 μl of an internal standard was added at a concentration of 100 ng/ml (186006963, Waters). The mixture was centrifuged at 4°C for 5 min at 8000*g*. After transferring to sterile plastic microtubes, the supernatant was evaporated until completely dry and then reconstituted in 100 μl of 80% (v/v) methanol and passed through a 0.22-μm membrane filter for LC-MS/MS analysis.

Protein stability analysis

The full-length coding sequence of *SlIAA32* was amplified by PCR from WT cDNA and cloned into the pET30a vector. The primers can be found in data S7. Protein production was induced as above. Recombinant SlIAA32-His was purified using Ni-NTA agarose (Beyotime, P2241). For cell-free degradation assays, total protein extracts were prepared from AZs treated with water only (negative control), NAA (50 μg/g; Sigma-Aldrich, 317918), or 10 μM L-Kyn (Sigma-Aldrich, K8625) using protein extraction buffer (25 mM

tris-HCl, pH 7.5, 10 mM NaCl, 10 mM $MgCl_2$, 4 mM PMSF, 5 mM dithiothreitol, and 10 mM adenosine triphosphate). Protein concentration was determined with a bicinchoninic acid (BCA) kit (Thermo Fisher Scientific, 23227). Each cell-free degradation reaction contained 500 μg of total proteins and 100 ng of recombinant SlIAA32-His. Aliquots of the mixtures were collected after incubation at 28°C for 0, 30, or 60 min. Immunoblotting with anti-His antibodies was used to determine the amount of SlIAA32-His remaining at each time point. For in vivo protein stability assays, total protein was extracted from AZ in WT, *SlLAX2*-OE, and *Sllax2* lines, then separated by SDS-PAGE. ACTIN was used as the loading control, which was detected by immunoblotting with anti-ACTIN antibodies. The relative band intensity was determined using ImageJ software (https://imagej.net/ij/). The protein content of the 0-hour sample was set to 1.

Immunofluorescence analysis

IAA distribution was determined as previously described (*45*). Freshly prepared AZ samples were prefixed for 2 hours in 3% (w/v) 1-ethyl-3-carbodiimide (Sigma-Aldrich, 341006) at 28°C before being transferred to FAA (Servicebio, G1108). The samples were dehydrated through a graded ethanol series (30, 50, 70, 80, 90, and 100%, all v/v). After dehydration, the samples were immersed in xylene and then Paraplast (Thermo Fisher Scientific) for 1 hour each time before embedding in 100% (w/v) Paraplast. The embedded samples were sliced into 10-mm slices. The sections were incubated with 1:100 (v/v) dilutions of anti-IAA monoclonal antibody (Sigma-Aldrich, A0855) at 4°C (12 to 16 hours), followed by Alexa Fluor 488–labeled anti-mouse IgG antibody [1:400 (v/v), Servicebio, GB25301] for 1 hour at room temperature in the dark. For cell wall staining, sections were immersed in 0.01% CFW (18909; Sigma-Aldrich) and subjected to dark treatment for 5 to 10 min before observation. The fluorescence signals were captured with an ortho-fluorescent microscope (Nikon), with an excitation wavelength of 465 to 495 nm and an emission wavelength of 515 to 555 nm (for IAA) and an excitation wavelength of 355 nm and an emission wavelength of 440 nm (for CFW).

For SlIAA3/SlIAA32 double immunofluorescence, the sections were incubated overnight with 1:300 (v/v) dilutions of anti-mCherry antibody and 1:200 (v/v) dilution of anti-SlIAA32 antibody at 4°C, followed by incubation with CY3-labeled anti-mouse IgG antibody [1:300 (v/v), Servicebio, GB21301] and Alexa Fluor 488–labeled anti-rabbit IgG antibody [1:400 (v/v), Servicebio, GB25303] for 1 hour at room temperature in the dark. For nucleus staining, sections were immersed in DAPI and subjected to dark treatment for 5 to 10 min before observation, with excitation/emission wavelengths of 587 nm/610 nm (DAPI). The fluorescence signals were captured with an ortho-fluorescent microscope (Nikon), with an excitation wavelength of 465 to 495 nm and an emission wavelength of 515 to 555 nm for Alexa Fluor 488 detection (for SlIAA32) and an excitation wavelength of 510 to 560 nm and an emission wavelength of 590 nm for mCherry (for SlIAA3). All fluorescence intensities were quantified by ImageJ. Measurements of fluorescence intensity were made for the longitudinal sections of tomato pedicel that extended from the proximal side of the AZ to the distal side over a distance of 200 μm. Within each 10-μm-length range, randomly choose 10 to 20 nuclear signals for measurement, then note the average value of each signal as the measurement result. The region between the pith and the epidermis was uniformly separated into nine layers for the cross-sectional slices, and the fluorescence intensity of each layer was assessed independently. Each experiment comprised 6 to 10 biological replicates.

LC-MS/MS analysis

LC-MS/MS analysis was used to identify which SlARF proteins were specifically enriched in pedicel AZs. The experiment was carried out with reference to previous studies (*59*). Total protein was extracted from AC AZs in protein lysate buffer [100 mM NH_4HCO_3, pH 8, 8 M urea, and 0.2% (w/v) SDS]. A total of 5 mg of total protein was digested with 1 ml of 50 mM NH_4HCO_3 containing 50 μg of Lys-C/trypsin protease mix (Promega, Madison, WI) at 37°C for 12 to 16 hours. All peptides were purified using StageTips (Thermo Fisher Scientific, 87782) before being analyzed by LC-MS/MS. Peptide concentration was determined using a BCA assay. Shotgun proteomics analysis was conducted using an EASY-nLCTM 1200 UHPLC system (Thermo Fisher Scientific) and a Q Exactive HF-X mass spectrometer (Thermo Fisher Scientific) in data-dependent acquisition mode. The raw files were processed using Proteome Discoverer software (Thermo Fisher Scientific, version 2.4) retrieval (MS1 tolerance, 10 ppm; MS2 tolerance, 0.02 Da; missed cleavage, 2). The peptide fragments were searched against the NCBI database (https://ncbi.nlm.nih.gov/).

ChIP-qPCR

The ChIP assays were conducted in accordance with previous methods (*60*). A total of 1 g of AZ tissue was collected from AC, *SlGATA6-Flag* OE, and *SlGATA6-Flag* OE *SlKD1*-RNAi plants. The obtained tissue samples were then cross-linked under vacuum in 3% (w/v) formaldehyde. The chromatin was fragmented to an average size of roughly 500 bp using a sonicator (Sonic Ruptor 400, Omni, USA). Immunoprecipitation was performed using 20 μl of anti-Flag antibody (CST, #14793). Following the collection of immunoprecipitated proteins using protein A beads (Thermo Fisher Scientific, 80103G), proteins were removed using proteinase K digestion (Thermo Fisher Scientific, 26160), followed by reverse cross-linking. The quantification of the immunoprecipitated DNA was performed using qPCR with SYBR Green dye on a qTOWER3/G real-time system (Analytik Jena). The primers can be found in data S7.

Laser microdissection and gene expression analysis

The laser microdissection experiments were performed following our previous methods (*61*). Laser microdissection was performed using a PALM MicroBeam system (Carl Zeiss, Germany). The frozen sections (10 μm) of WT and *SlKD1*-RNAi AZs were placed on the MembraneSlide 1.0 PEN (Zeiss, No. 415101-4401-000). Incubate the sections in ice-cold 100% ethanol for 2 to 3 min to dehydrate. Specific pedicel tissue sections (distal side of AZ, AZ, and proximal side of AZ) were removed from tissue slices ($n = 5$) and collected in AdhesiveCap 500 tubes (Zeiss). The tubes were frozen in liquid nitrogen and stored at −80°C. Total RNA was extracted from tissue samples using the RNeasy Micro Kit (Qiagen), following the manufacturer's instructions. Then, RT-qPCR analysis was conducted on the isolated RNA following the previously outlined methods.

Statistical analysis

Experiments were conducted with three separate biological replicates unless noted otherwise. The figures or figure legends include specific statistical parameters for each experiment. Statistical analyses were performed using GraphPad Prism (v9).

Accession numbers

Sequence data from this article can be found in Sol Genomics Network (https://solgenomics.net/) or NCBI (https://ncbi.nlm.nih.gov/) under the accession numbers listed in data S7.

Supplementary Materials

The PDF file includes:

Figs. S1 to S19

Legends for data S1 to S7

Other Supplementary Material for this manuscript includes the following:

Data S1 to S7

REFERENCES AND NOTES

1. H. P. Rasmussen, M. J. Bukovac, Naphthaleneacetic acid: Localization in the abscission zone of the bean. *Science* **152**, 217–218 (1966).
2. L. Mao, D. Begum, H. W. Chuang, M. A. Budiman, E. J. Szymkowiak, E. E. Irish, R. A. Wing, JOINTLESS is a MADS-box gene controlling tomato flower abscission zone development. *Nature* **406**, 910–913 (2000).
3. S. Meir, S. Philosoph-Hadas, S. Sundaresan, K. S. Selvaraj, S. Burd, R. Ophir, B. Kochanek, M. S. Reid, C. Z. Jiang, A. Lers, Microarray analysis of the abscission-related transcriptome in the tomato flower abscission zone in response to auxin depletion. *Plant Physiol.* **154**, 1929–1956 (2010).
4. B. Rubinstein, A. C. Leopold, Analysis of the auxin control of bean leaf abscission 12. *Plant Physiol.* **38**, 262–267 (1963).
5. S. Meir, D. A. Hunter, J.-C. Chen, V. Halaly, M. S. Reid, Molecular changes occurring during acquisition of abscission competence following auxin depletion in *Mirabilis jalapa*. *Plant Physiol.* **141**, 1604–1616 (2006).
6. F. B. Abeles, B. Rubinstein, Regulation of ethylene evolution and leaf abscission by auxin 1. *Plant Physiol.* **39**, 963–969 (1964).
7. M. M. Basu, Z. H. González-Carranza, S. Azam-Ali, S. Tang, A. A. Shahid, J. A. Roberts, The manipulation of auxin in the abscission zone cells of *Arabidopsis* flowers reveals that indoleacetic acid signaling is a prerequisite for organ shedding. *Plant Physiol.* **162**, 96–106 (2013).
8. M. Jacobs, P. H. Rubery, Naturally occurring auxin transport regulators. *Science* **241**, 346–349 (1988).
9. F. T. Addicott, R. S. Lynch, H. R. Carns, Auxin gradient theory of abscission. *Regulation* **121**, 644–645 (1955).
10. O. R. Patharkar, J. C. Walker, Advances in abscission signaling. *J. Exp. Bot.* **69**, 733–740 (2017).
11. R. Li, C.-L. Shi, X. Wang, Y. Meng, L. Cheng, C.-Z. Jiang, M. Qi, T. Xu, T. Li, Inflorescence abscission protein SlIDL6 promotes low light intensity-induced tomato flower abscission. *Plant Physiol.* **186**, 1288–1301 (2021).
12. L. Cheng, R. Li, X. Wang, S. Ge, S. Wang, X. Liu, J. He, C. Z. Jiang, M. Qi, T. Xu, T. Li, A SlCLV3-SlWUS module regulates auxin and ethylene homeostasis in low light-induced tomato flower abscission. *Plant Cell* **34**, 4388–4408 (2022).
13. S. Reichardt, H.-P. Piepho, A. Stintzi, A. Schaller, Peptide signaling for drought-induced tomato flower drop. *Science* **367**, 1482–1485 (2020).
14. R. J. Pattison, C. Catalá, Evaluating auxin distribution in tomato (*Solanum lycopersicum*) through an analysis of the PIN and AUX/LAX gene families. *Plant J.* **70**, 585–598 (2012).
15. B. Péret, K. Swarup, A. Ferguson, M. Seth, Y. Yang, S. Dhondt, N. James, I. Casimiro, P. Perry, A. Syed, H. Yang, J. Reemmer, E. Venison, C. Howells, M. A. Perez-Amador, J. Yun, J. Alonso, G. T. Beemster, L. Laplaze, A. Murphy, M. J. Bennett, E. Nielsen, R. Swarup, AUX/LAX genes encode a family of auxin influx transporters that perform distinct functions during *Arabidopsis* development. *Plant Cell* **24**, 2874–2885 (2012).
16. L. Gälweiler, C. Guan, A. Müller, E. Wisman, K. Mendgen, A. Yephremov, K. Palme, Regulation of polar auxin transport by AtPIN1 in *Arabidopsis* vascular tissue. *Science* **282**, 2226–2230 (1998).
17. J. Petrásek, J. Mravec, R. Bouchard, J. J. Blakeslee, M. Abas, D. Seifertová, J. Wisniewska, Z. Tadele, M. Kubes, M. Covanová, P. Dhonukshe, P. Skupa, E. Benková, L. Perry, P. Krecek, O. R. Lee, G. R. Fink, M. Geisler, A. S. Murphy, C. Luschnig, E. Zazímalová, J. Friml, PIN proteins perform a rate-limiting function in cellular auxin efflux. *Science* **312**, 914–918 (2006).
18. Z. Shi, Y. Jiang, X. Han, X. Liu, R. Cao, M. Qi, T. Xu, T. Li, SlPIN1 regulates auxin efflux to affect flower abscission process. *Sci. Rep.* **7**, 14919 (2017).
19. S. Vanneste, J. Friml, Auxin: A trigger for change in plant development. *Cell* **136**, 1005–1016 (2009).
20. M. Cao, R. Chen, P. Li, Y. Yu, R. Zheng, D. Ge, W. Zheng, X. Wang, Y. Gu, Z. Gelová, J. Friml, H. Zhang, R. Liu, J. He, T. Xu, TMK1-mediated auxin signalling regulates differential growth of the apical hook. *Nature* **568**, 240–243 (2019).
21. R. Sager, X. Wang, K. Hill, B.-C. Yoo, J. Caplan, A. Nedo, T. Tran, M. J. Bennett, J.-Y. Lee, Auxin-dependent control of a plasmodesmal regulator creates a negative feedback loop modulating lateral root emergence. *Nat. Commun.* **11**, 364 (2020).
22. C. M. Ellis, P. Nagpal, J. C. Young, G. Hagen, T. J. Guilfoyle, J. W. Reed, *AUXIN RESPONSE FACTOR1* and *AUXIN RESPONSE FACTOR2* regulate senescence and floral organ abscission in *Arabidopsis thaliana*. *Development* **132**, 4563–4574 (2005).
23. Y. Okushima, I. Mitina, H. L. Quach, A. Theologis, AUXIN RESPONSE FACTOR 2 (ARF2): A pleiotropic developmental regulator. *Plant J.* **43**, 29–46 (2005).
24. B. Abebie, A. Lers, S. Philosoph-Hadas, R. Goren, J. Riov, S. Meir, Differential effects of NAA and 2,4-D in reducing floret abscission in cestrum (*Cestrum elegans*) cut flowers are associated with their differential activation of Aux/IAA homologous genes. *Ann. Bot.* **101**, 249–259 (2008).
25. Y. Gao, C. Liu, X. Li, H. Xu, Y. Liang, N. Ma, Z. Fei, J. Gao, C. Z. Jiang, C. Ma, Transcriptome profiling of petal abscission zone and functional analysis of an Aux/IAA family gene RhIAA16 involved in petal shedding in rose. *Front. Plant Sci.* **7**, 1375 (2016).
26. J. C. Reyes, M. I. Muro-Pastor, F. J. Florencio, The GATA family of transcription factors in *Arabidopsis* and rice. *Plant Physiol.* **134**, 1718–1732 (2004).
27. Q. Yuan, C. Zhang, T. Zhao, M. Yao, X. Xu, A genome-wide analysis of GATA transcription factor family in tomato and analysis of expression patterns. *Int. J. Agric. Biol.* **20**, 1274–1282 (2018).
28. K. Jiang, V. Yung, T. Chiba, L. J. Feldman, Longitudinal patterning in roots: A GATA2-auxin interaction underlies and maintains the root transition domain. *Planta* **247**, 831–843 (2018).
29. X.-M. Luo, W.-H. Lin, S. Zhu, J.-Y. Zhu, Y. Sun, X.-Y. Fan, M. Cheng, Y. Hao, E. Oh, M. Tian, L. Liu, M. Zhang, Q. Xie, K. Chong, Z.-Y. Wang, Integration of light- and brassinosteroid-signaling pathways by a GATA transcription factor in *Arabidopsis*. *Dev. Cell* **19**, 872–883 (2010).
30. Y. Wang, X. Cao, D. Zhang, Y. Li, Q. Wang, F. Ma, X. Xu, X. Zhan, T. Hu, SlGATA17, a tomato GATA protein, interacts with SlHY5 to modulate salinity tolerance and germination. *Environ. Exp. Bot.* **206**, 105191 (2023).
31. A. Hay, M. Tsiantis, KNOX genes: Versatile regulators of plant development and diversity. *Development* **137**, 3153–3165 (2010).
32. C. Ma, S. Meir, L. Xiao, J. Tong, Q. Liu, M. S. Reid, C.-Z. Jiang, A KNOTTED1-LIKE HOMEOBOX protein regulates abscission in tomato by modulating the auxin pathway. *Plant Physiol.* **167**, 844–853 (2015).
33. S. Sundaresan, S. Philosoph-Hadas, C. Ma, C. Z. Jiang, J. Riov, B. Kochanek, S. Salim, M. S. Reid, S. Meir, Role of the KNOTTED1-LIKE HOMEOBOX protein (KD1) in regulating abscission of tomato flower pedicels at early and late stages of the process. *Physiol. Plant.* **173**, 2103–2118 (2021).
34. A. Bartlett, R. C. O'Malley, S.-s. C. Huang, M. Galli, J. R. Nery, A. Gallavotti, J. R. Ecker, Mapping genome-wide transcription-factor binding sites using DAP-seq. *Nat. Protoc.* **12**, 1659–1672 (2017).
35. R. C. O'Malley, S. C. Huang, L. Song, M. G. Lewsey, A. Bartlett, J. R. Nery, M. Galli, A. Gallavotti, J. R. Ecker, Cistrome and epicistrome features shape the regulatory DNA landscape. *Cell* **165**, 1280–1292 (2016).
36. T. Ulmasov, J. Murfett, G. Hagen, T. J. Guilfoyle, Aux/IAA proteins repress expression of reporter genes containing natural and highly active synthetic auxin response elements. *Plant Cell* **9**, 1963–1971 (1997).
37. S. B. Tiwari, G. Hagen, T. J. Guilfoyle, Aux/IAA proteins contain a potent transcriptional repression domain. *Plant Cell* **16**, 533–543 (2004).
38. W. M. Gray, S. Kepinski, D. Rouse, O. Leyser, M. Estelle, Auxin regulates SCFTIR1-dependent degradation of AUX/IAA proteins. *Nature* **414**, 271–276 (2001).
39. C. Audran-Delalande, C. Bassa, I. Mila, F. Regad, M. Zouine, M. Bouzayen, Genome-wide identification, functional analysis and expression profiling of the Aux/IAA gene family in tomato. *Plant Cell Physiol.* **53**, 659–672 (2012).
40. T. Ulmasov, G. Hagen, T. J. Guilfoyle, ARF1, a transcription factor that binds to auxin response elemets. *Science* **276**, 1865–1868 (1997).
41. A. Israeli, J. W. Reed, N. Ori, Genetic dissection of the auxin response network. *Nat. Plants* **6**, 1082–1090 (2020).
42. D. A.Breitel, L. Chappell-Maor, S. Meir, I. Panizel, C. P. Puig, Y. Hao, T. Yifhar, H. Yasuor, M. Zouine, M. Bouzayen, A. Granell Richart, I. Rogachev, A. Aharoni, AUXIN RESPONSE FACT OR 2 Intersects Hormonal Signals in the Regulation of Tomato Fruit Ripening. *PLOS Genet.* **12**, e1005903 (2016). https://doi.org/10.1371/journal.pgen.1005903.
43. B. Orosa-Puente, N. Leftley, D. von Wangenheim, J. Banda, A. K. Srivastava, K. Hill, J. Truskina, R. Bhosale, E. Morris, M. Srivastava, B. Kümpers, T. Goh, H. Fukaki, J. E. M. Vermeer, T. Vernoux, J. R. Dinneny, A. P. French, A. Bishopp, A. Sadanandom, M. J. Bennett, Root branching toward water involves posttranslational modification of transcription factor ARF7. *Science* **362**, 1407–1410 (2018).
44. E. Shani, M. Salehin, Y. Zhang, S. E. Sanchez, C. Doherty, R. Wang, C. C. Mangado, L. Song, I. Tal, O. Pisanty, J. R. Ecker, S. A. Kay, J. Pruneda-Paz, M. Estelle, Plant stress tolerance requires auxin-sensitive Aux/IAA transcriptional repressors. *Curr. Biol.* **27**, 437–444 (2017).

45. Y. Liang, C. Jiang, Y. Liu, Y. Gao, J. Lu, P. Aiwaili, Z. Fei, C. Z. Jiang, B. Hong, C. Ma, J. Gao, Auxin regulates sucrose transport to repress petal abscission in rose (*Rosa hybrida*). *Plant Cell* **32**, 3485–3499 (2020).
46. X. Dong, C. Ma, T. Xu, M. S. Reid, C.-Z. Jiang, T. Li, Auxin response and transport during induction of pedicel abscission in tomato. *Hort Res.* **8**, 192 (2021).
47. D. S. Louie, F. T. Addicott, Applied auxin gradients and abscission in explants. *Plant Physiol.* **45**, 654–657 (1970).
48. Y. Mao, H. Zhang, N. Xu, B. Zhang, F. Gou, J. K. Zhu, Application of the CRISPR-Cas system for efficient genome engineering in plants. *Mol. Plant* **6**, 2008–2011 (2013).
49. Y. Wang, T. Li, H. Meng, X. Sun, Optimal and spatial analysis of hormones, degrading enzymes and isozyme profiles in tomato pedicel explants during ethylene-induced abscission. *Plant Growth Regul.* **46**, 97–107 (2005).
50. D. Q. Fu, B. Z. Zhu, H. L. Zhu, W. B. Jiang, Y. B. Luo, Virus-induced gene silencing in tomato fruit. *Plant J.* **43**, 299–308 (2005).
51. H. Liu, D. Fu, B. Zhu, H. Yan, X. Shen, J. Zuo, Y. Zhu, Y. Luo, Virus-induced gene silencing in eggplant (*Solanum melongena*). *J. Integr. Plant Biol.* **54**, 422–429 (2012).
52. H. X. Yan, D. Q. Fu, B. Z. Zhu, H. P. Liu, X. Y. Shen, Y. B. Luo, Sprout vacuum-infiltration: A simple and efficient agroinoculation method for virus-induced gene silencing in diverse solanaceous species. *Plant Cell Rep.* **31**, 1713–1722 (2012).
53. Y. Liu, M. Schiff, S. P. Dinesh-Kumar, Virus-induced gene silencing in tomato. *Plant J.* **31**, 777–786 (2002).
54. R. González-Lamothe, P. Boyle, A. Dulude, V. Roy, C. Lezin-Doumbou, G. S. Kaur, K. Bouarab, C. Després, N. Brisson, The transcriptional activator Pti4 is required for the recruitment of a repressosome nucleated by repressor SEBF at the potato PR-10a gene. *Plant Cell* **20**, 3136–3147 (2008).
55. K. J. Livak, T. D. Schmittgen, Analysis of relative gene expression data using real-time quantitative PCR and the $2^{-\Delta\Delta CT}$ method. *Methods* **25**, 402–408 (2001).
56. H. Irieda, Y. Takano, Epidermal chloroplasts are defense-related motile organelles equipped with plant immune components. *Nat. Commun.* **12**, 2739 (2021).
57. Y. Wang, W. Zou, Y. Xiao, L. Cheng, Y. Liu, S. Gao, Z. Shi, Y. Jiang, M. Qi, T. Xu, T. Li, MicroRNA1917 targets CTR4 splice variants to regulate ethylene responses in tomato. *J. Exp. Biol.* **69**, 1011–1025 (2018).
58. X. Dong, X. Liu, L. Cheng, R. Li, S. Ge, S. Wang, Y. Cai, Y. Liu, S. Meng, C.-Z. Jiang, C.-L. Shi, T. Li, D. Fu, M. Qi, T. Xu, SlBEL11 regulates flavonoid biosynthesis, thus fine-tuning auxin efflux to prevent premature fruit drop in tomato. *J. Integr. Plant Biol.* **66**, 749–770 (2024).
59. S. Yang, W. Cai, R. Wu, Y. Huang, Q. Lu, W. Hui, X. Huang, Y. Zhang, Q. Wu, X. Cheng, M. Wan, J. Lv, Q. Liu, X. Zheng, S. Mou, D. Guan, S. He, Differential CaKAN3-CaHSF8 associations underlie distinct immune and heat responses under high temperature and high humidity conditions. *Nat. Commun.* **14**, 4477 (2023).
60. X. Liu, L. Cheng, R. Li, Y. Cai, X. Wang, X. Fu, X. Dong, M. Qi, C. Z. Jiang, T. Xu, T. Li, The HD-Zip transcription factor SlHB15A regulates abscission by modulating jasmonoyl-isoleucine biosynthesis. *Plant Physiol.* **189**, 2396–2412 (2022).
61. R. Wang, R. Li, L. Cheng, X. Wang, X. Fu, X. Dong, M. Qi, C. Jiang, T. Xu, T. Li, SlERF52 regulates SlTIP1;1 expression to accelerate tomato pedicel abscission. *Plant Physiol.* **185**, 1829–1846 (2021).
62. C. Chen, H. Chen, Y. Zhang, H. R. Thomas, M. H. Frank, Y. He, R. Xia, TBtools: An integrative toolkit developed for interactive analyses of big biological data. *Mol. Plant* **13**, 1194–1202 (2020).

Acknowledgments

Funding: This work was supported by the National Natural Science Foundation of China (grants 32330097, 32372687, and 32302645). **Author contributions:** Conceptualization: T.X. Methodology: T.X., T.L., and C.-Z.J. Investigation: Xianfeng Liu, L.C., Y.C., Y.L., X.Y., J.L., R.L., S.G., S.W., Xingan Liu, S.M., and M.Q. Visualization: Xianfeng Liu. Supervision: T.X. and T.L. Writing—original draft: T.X. and Xianfeng Liu. Writing—review and editing: T.X. and Xianfeng Liu. **Competing interests:** The authors declare that they have no competing interests. **Data and materials availability:** The RNA-seq and DAP-seq data from this study have been deposited with the National Center for Biotechnology Information under the following accession numbers: PRJNA1196094 and PRJNA1196314. All other data needed to evaluate the conclusions in the paper are present in the paper and/or the Supplementary Materials.

Submitted 16 September 2024
Accepted 12 February 2025
Published 19 March 2025
10.1126/sciadv.adt1891